Tsunami Hazards Associated with the Catalina Fault in Southern California

Mark R. Legg,[a] M.EERI, Jose C. Borrero,[b] and Costas E. Synolakis[b]

We investigate the tsunami hazard associated with the Catalina Fault offshore of southern California. Realistic faulting parameters are used to match coseismic displacements to existing sea floor topography. Several earthquake scenarios with moment magnitudes ranging between 7.0 and 7.6 are used as initial conditions for tsunami simulations, which predict runup of up to 4 m. Normalizing runup with the maximum uplift identifies areas susceptible to tsunami focusing and amplification. Several harbors and ports in southern California lie in areas where models predict tsunami amplification. Return periods are estimated by dividing the modeled seafloor uplift per event by the observed total uplift of the Santa Catalina Island platform multiplied by the time since the uplift began. The analysis yields return periods between 2,000 to 5,000 years for the Catalina Fault alone, and 200 to 500 years when all offshore faults are considered. [DOI: 10.1193/1.1773592]

INTRODUCTION

Locally generated tsunamis from major active faults offshore southern California threaten nearby coastal cities. Disruption of operations at port facilities due to tsunami attack could severely impact the regional and national economies. Historically, the potential for tsunami generation from local sources was believed to be insignificant because most of the faulting in the southern California region is strike-slip in character. Yet major thrust and reverse faulting occurs throughout the western Transverse Ranges (WTR), including historical tsunami occurrence following strong earthquakes in the Santa Barbara Channel region and west of Point Conception (McCulloch 1985, Lander et al. 1993, McCarthy et al. 1993, Borrero et al. 2001). Furthermore, the major strike-slip faults offshore southern California, south of the WTR, have sinuous traces with many bends and step-overs. Local tectonic convergence at restraining bends and step-overs creates folding and seafloor uplift, whereas tectonic divergence at releasing bends and step-overs produces extension and seafloor subsidence (Legg and Kennedy 1991). Rapid seafloor deformation at these fault bends and offsets may, in principle, generate damaging local tsunamis. Here we examine the large seafloor uplift of the Santa Catalina Island platform (Figure 1), and its potential for generating destructive local tsunamis in the southern California coastal area.

[a] Legg Geophysical, 16541 Gothard Street, #107, Huntington Beach, CA 92647
[b] Dept. Civil and Aerospace Engineering, University of Southern California, Los Angeles, CA 90089-2531

Earthquake Spectra, Volume 20, No. 3, pages 1–34, August 2004;

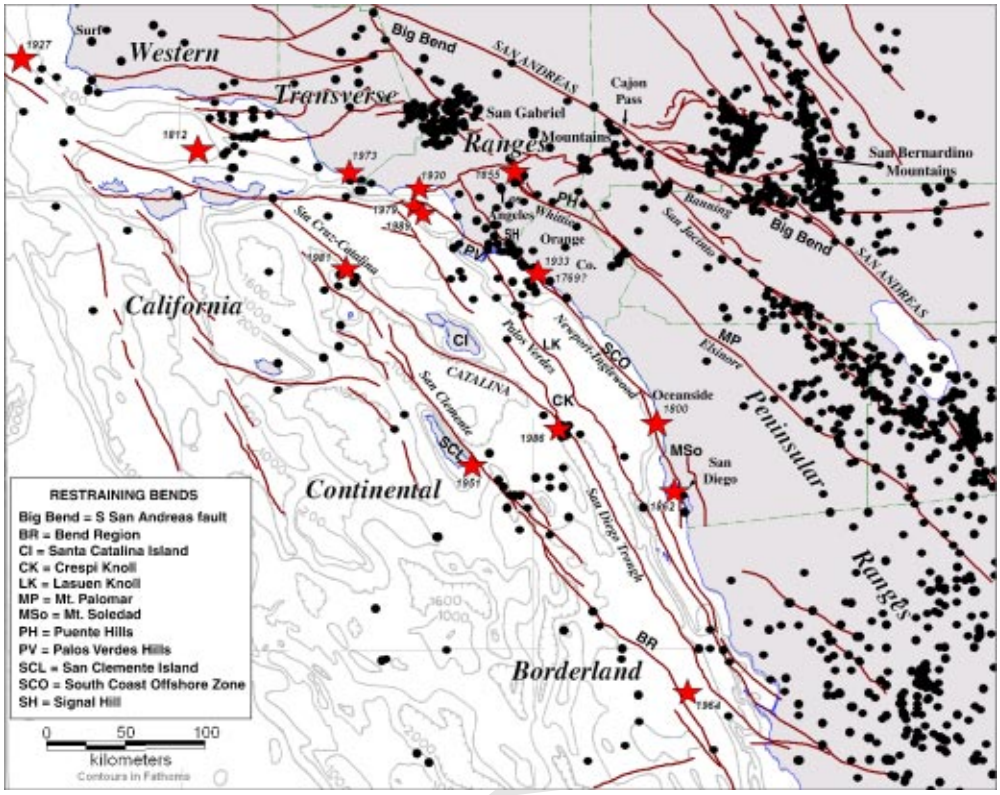

Figure 1. Map showing major faults and recent seismicity (magnitude≥4) of the southern California coastal and offshore region. Epicenters from Southern California Seismograph Network (1932–1998) are shown as small circles; significant offshore historical events are shown as stars. Prominent restraining bends along the major right-slip faults of the region are also identified.

SOUTHERN CALIFORNIA OFFSHORE FAULTING AND TECTONICS

The submarine area west of southern California is called the California Continental Borderland (Shepard and Emery 1941). The physiography of the Borderland consists of generally northwest-trending ridges, banks, and basins, considered to represent a submerged equivalent of the Peninsular Ranges (Moore 1969). More recent studies, however, show that Borderland geologic structure and physiography is rather similar to the Basin and Range province (Legg 1991). This ridge and basin structure persists as the San Andreas fault system accommodates about 52±2 mm/yr of right shear between the Pacific and North America tectonic plates (DeMets and Dixon 1999). A significant component of the relative motion, perhaps as much as 20% (10–11 mm/yr), occurs on faults west of the southern California coastline (Legg 1991, Larson 1993, Bennett et al. 1996). Oblique-slip on curvilinear and offset fault segments locally maintains or enhances the inherited structural relief and Borderland physiography.

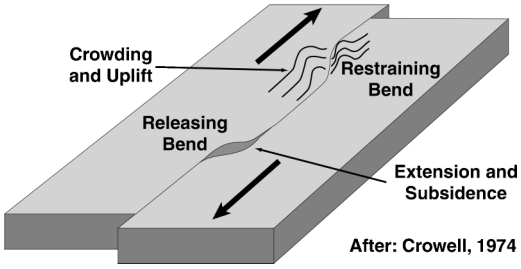

Figure 2. Material crowded into a restraining bend along a strike-slip fault results in convergence, folding and reverse faulting that creates a local uplift. In contrast, extension and subsidence occurs at a releasing bend.

Like the San Andreas, major faults offshore southern California with northwest trends are right-slip in character (Vedder et al. 1974, 1986; Clarke et al. 1987; Legg et al. 1989). Offshore faults with east-west trends lie generally within or along the edge of the WTR and show thrust, reverse, or left-slip character. Vertical deformation occurring along coastal and offshore fault zones is directly responsible for uplift of coastal and island marine terraces (Lajoie et al. 1992). Uplifted marine terraces are prominent, not only within the WTR where major folding and thrust faulting occurs, but also along the southern California coast where right-slip faulting predominates. Relative uplift or subsidence of the latest Pleistocene lowstand shoreline (18 ka) is suggested in warping of this regional submerged marine terrace platform (Goldfinger et al. 2003). Rapid coseismic seafloor uplift or subsidence along major Borderland fault zones may produce destructive tsunamis during large submarine earthquakes.

RESTRAINING BENDS: POP-UPS AND PULL-APARTS

The sinuosity and en echelon character of real strike-slip faults produces local areas of convergence and divergence (Figure 2; Crowell 1974), with local uplifts at restraining bends and subsiding pull-apart basins at releasing offsets. For right-lateral faults common to southern California, a bend or step to the right in the fault trace results in an area of divergence and subsidence, whereas a bend or step to the left results in an area of convergence with local folding and uplift. Rapid vertical seafloor deformation during large earthquakes at these fault irregularities may generate a local tsunami, while long-term oblique deformation at these irregularities may form deep, sediment-filled pull-apart or sag basins along extensional (transtensional) fault segments and elevated submarine ridges or islands at major restraining (transpressional) segments.

Numerous features on the seafloor offshore southern California may be attributed to oblique deformation along the major right-slip fault zones of the Inner Borderland (Figure 1). It appears that for every restraining bend uplift there is a related releasing bend sag or pull-apart basin (Legg et al. 1999). Rotation of crustal blocks in these zones of simple shear further accentuates fault irregularities, for example, the large-scale clockwise rotation of the WTR since middle Miocene time (Kamerling and Luyendyk 1979, Luyendyk 1991). The resulting zone of north-directed convergence at the southern

boundary of the WTR likely enhances the formation of restraining bends and transpressional uplift apparent in the northern Borderland (Figure 1). Yet prominent northwest-trending ridges such as the Santa Cruz–Catalina Ridge, and recent earthquakes with thrust fault mechanisms on northwest-trending fault planes, such as the 1986 Oceanside event (Hauksson and Jones 1988) suggest that north-south principal shortening rotates into northeast-directed shortening farther south and east along coastal and offshore southern California. Large-scale evidence of this northeast-directed convergence may be apparent in the thrust reactivation of the regional Oceanside detachment fault system (Crouch and Suppe 1993, Rivero et al. 2000). Strain partitioning likely occurs with right-slip accommodated on the vertical or high-angle northwest-trending faults and thrusting or oblique-reverse faulting on the low to moderate dipping faults (Nicholson and Crouch 1989).

Uplifts at strike-slip fault restraining bends are called "pop-ups" (cf., McClay and Bonora 2001). Analog modeling of restraining bends and step-overs along strike-slip faults show a general rhomboid-shaped uplift pattern with numerous secondary and branch faults bounding and within the pop-up (McClay and Bonora 2001). The equivalent subsiding extensional structure at the idealized pull-apart basin is called a "rhombochasm" (Crowell 1974). Several restraining bend pop-up structures identified within the Inner Borderland show the rhomboid shape (Figure 1) at scales ranging from a few kilometers wide and several kilometers long (offshore west of Oceanside) to more than 20 kilometers wide by 80 kilometers long (Santa Catalina Island platform). Structural relief on these features ranges from a few hundred meters to more than two kilometers (Vedder 1987, Legg and Kennedy 1991).

Restraining bend pop-ups are observed onshore in southern California as well. Examples include Signal Hill along the Newport-Inglewood fault zone in the Los Angeles Basin, Mount Soledad along the Rose Canyon Fault in La Jolla (San Diego), and possibly the San Bernardino Mountains along the San Andreas Fault or the San Gabriel Mountains along the San Gabriel Fault (Figure 1; Morton and Matti 1993; Weldon et al. 1993). Indeed, the largest restraining bend known in the region is the "Big Bend" along the southern San Andreas Fault, located between the Salton Trough and the California Coast Ranges (Figure 1).

SOUTHERN CALIFORNIA OFFSHORE EARTHQUAKE AND TSUNAMI HISTORY

Southern California has suffered severe offshore earthquakes and tsunamis in its brief ~200-year recorded history (Table 1; Appendix). Damage was minor from these events, due to the sparse population of the region in the early years and lack of large events (moment magnitude, $M_W \geq 7$) during the more recent period of substantial population growth. Moderate earthquakes in 1981 and 1986 have ruptured the faults at opposite ends of the Catalina Fault. Furthermore, two large strike-slip earthquakes ($M_W > 7$) have occurred within the past decade on low-slip rate faults of the Mojave Desert region, which has similar geologic structure and tectonic style to the offshore Borderland. The 1989 Loma Prieta earthquake ($M_W = 6.9$) demonstrated that oblique reverse earthquakes along restraining bends of the San Andreas Fault system in coastal areas can generate local tsunamis (Schwing et al. 1990). The shaking from a large earthquake

Table 1. Possible locally generated tsunami along the southern California coast

Date (UTC)	Magnitude	Area Affected	Waves Reported
1806 May 25	?	Santa Barbara	Boats beached(?)
1812 Dec. 21	7–7½ (M_I)	Santa Barbara Channel	3- to 4-m runup at Gaviota
1854 May 31	?	Santa Barbara	Local inundation near embarcadero
1854 July 24	?	San Diego	0.1 m amplitude, 36 minutes period
1855 July 11	6 (M_I)	San Juan Capistrano	Two unusually heavy sea waves
1862 May 27	6.2 (M_I)	San Diego Bay	<1 m
1878 Nov 22	?	Central Coast	Damage at Point Sal, Cayucos, Avila
1879 Aug 10	?	Santa Monica Bay	?
1895 Mar 9	?	San Miguel Island	Disturbed water; coastal landslide(?)
1927 Nov 4	7.3 (M_S)	Point Arguello	1.8-m runup at Surf, 1.5-m runup at Port San Luis
1930 Aug 31	5.25 (M_W)	Santa Monica Bay	Local oscillations to about 0.6 m
1933 Mar 11	6.25 (M_W)	Long Beach	Uncertain records
1979 Jan 1	5.0 (M_L)	Santa Monica Bay	Local oscillations (?); no tsunami
1989 Jan 19	5.0 (M_L)	Santa Monica Bay	Local oscillations (?); no tsunami

Modified and updated from McCulloch (1985), Lander et al. (1993), McCarthy et al. (1993), Toppozada et al. (2000)

Magnitude Scale: M_W=Moment Magnitude; M_S=Surface Wave Magnitude; M_L=Local (Richter) Magnitude; M_I=Seismic Intensity Magnitude; ?=Magnitude Not Given or Unknown

($M_W \geq 7$) offshore southern California would damage coastal communities, and its effect would be enhanced were a tsunami triggered from the seafloor displacement.

EARTHQUAKE MODELING

Modeling of potential earthquake sources in the southern California offshore region is necessary to predict tsunamigenic seafloor deformations (Synolakis et al. 1997). Geometric irregularities along active strike-slip faults may produce significant seafloor uplift or subsidence. Increased normal stress upon the transpressional fault surface along a restraining bend may lock the fault and result in infrequent large earthquakes with relative quiescence in microseismicity during the interseismic period (Hill et al. 1990). This pattern has been inferred for the San Andreas Fault, where infrequent large earthquakes have been identified from paleoseismological investigations (Sieh et al. 1989). Assuming similar behavior for major offshore faults, the transpressional zones where large restraining bends occur may represent the sites of prehistoric and future large earthquakes ($M_W \geq 7$). Indeed, 70 years of seismicity data for southern California show few earthquakes along the Catalina Fault, yet moderate earthquakes ($M_W \sim 6$) with rich aftershock sequences struck the faults at the two ends of this seismic gap. Coseismic seafloor uplift associated with large offshore restraining bend earthquakes may generate destructive local tsunamis in the California Continental Borderland.

Major restraining bends in the area offshore southern California (Figure 1) include the Oceanside and Dana Point segments of the offshore Newport-Inglewood (South Coast Offshore) fault zone (Fischer and Mills 1991); the Palos Verdes Hills, offshore

Palos Verdes Anticlinorium, and Lasuen Knoll along the Palos Verdes fault zone (Nardin and Henyey 1978, Mann and Gordon 1996); the Santa Catalina Island platform along the San Diego Trough–Catalina fault zone (Junger 1976, Mann and Gordon 1996); the southern half of San Clemente Island; and the "Bend Region" of the San Clemente fault zone (Legg and Kennedy 1991, Legg et al. 1999). All of these features show folding and faulting of late Cenozoic, and locally, Holocene sediments, as well as seafloor uplift ranging from 10 m to more than 1 km (cf., Vedder et al. 1974, Vedder et al. 1986, Clarke et al. 1987).

In addition, numerous earthquakes have been located along these major fault zones, although epicenters are sparse along the restraining bend segments (Figure 1). Considering the length of the restraining bend fault segments (30–150 km) and the overall length of these fault zones (>100–300 km), numerous potential sources of large offshore tsunamigenic earthquakes can be inferred.

The Santa Catalina Island platform represents the largest restraining bend pop-up recognized in the northern California Continental Borderland (Figures 1 and 3). It lies within 50 km of the urban Los Angeles and Orange County coastline where it may produce damaging shaking intensities during large earthquakes. Its coast parallel orientation could direct tsunami energy selectively towards this heavily populated area.

ELASTIC DISLOCATION MODEL

Most studies of earthquake-generated tsunamis use elastic dislocation theory to predict the seafloor displacement based on fault rupture models (e.g., Satake and Somerville 1992, Geist 1998). Often these studies find that earthquake source models involving spatially uniform slip over a simple fault rupture surface underestimate the observed tsunami runup (Synolakis et al. 1997, Geist 2002). In some cases, other mechanisms, such as submarine landslides, may be invoked to produce the locally observed higher runup and inundation levels (Borrero et al. 2001, Synolakis et al. 2002). Although large earthquakes frequently generate substantial landslides in the epicentral area, this study focuses on tectonic deformation mechanisms from submarine strike-slip faulting.

As noted by Geist (2002), complex rupture processes have important effects on the tsunami generation and local runup. Real earthquakes have non-uniform slip distributions (e.g., Hartzell and Heaton 1983, Wald and Heaton 1994), often involving multiple fault segments (Sieh et al. 1993), and high slip patches (Geist 2002, Okal et al. 2002). To address these issues, we develop a multiple segment fault rupture and earthquake source model for tsunami generation. Because source complexities such as variable rigidity along the fault surface and highly irregular slip distributions are difficult to infer with limited subsurface data, our model retains the simplicity of uniform slip patches and constant rigidity, but uses several segments with different fault geometries and slip vectors.

For the tsunami model, the static vertical tectonic displacement is used to model initial wave heights. To calibrate this simple model to more realistic earthquake and faulting parameters, we attempt to match the three-dimensional shape of the long-term seafloor uplift observed at the Santa Catalina Island restraining bend (Figures 3 and 4; Legg and Borrero 2001). The elastic dislocation model is adjusted to produce a pattern of sea-

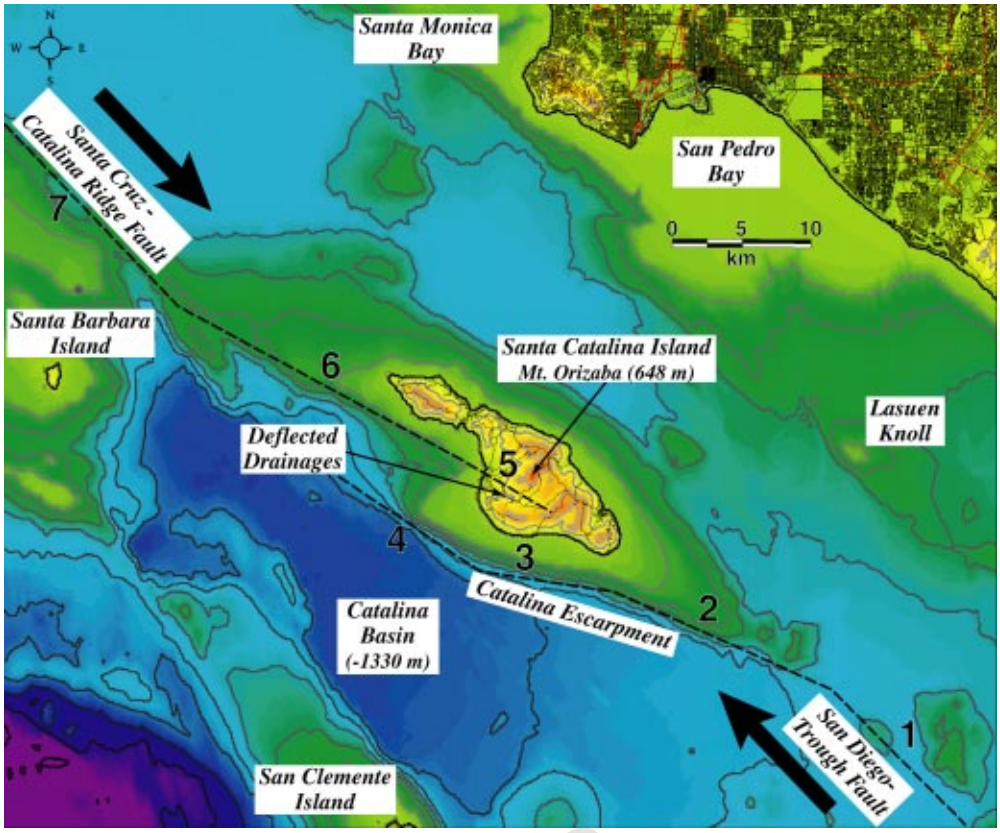

Figure 3. Contour map of the Santa Catalina Island "pop-up" structure. Seven segment Catalina Fault used for the tsunami earthquake models is shown. Large arrows show relative dextral motion across the Catalina Fault that creates transpression at the restraining bend. Deflected drainages suggest existence of right-slip fault aligned with the Santa Cruz–Catalina Ridge that cuts through the island.

floor uplift that mimics the shape of the uplift using fault displacements that are scaled to represent realistic values observed in other large earthquakes throughout California and the world (e.g., Wald and Heaton 1994, Wells and Coppersmith 1994).

Long-term post- and interseismic relaxation, plus loading due to sedimentation and erosion modify the uplift produced during the coseismic deformation. Although some models predict a broadening of the deformation, investigation of real earth structures find that coseismic deformation from recent large earthquakes is of comparable width to the overall structure, implying that the effective elastic thickness of the crust is small (King et al. 1988, Stein et al. 1988). For this study, the post- and interseismic loading effects are reduced. The Catalina basin to the southwest of the uplift is sediment starved, dominated by slow hemipelagic sedimentation (Vedder 1987), and submarine erosion of the uplift appears minor, as no large submarine landslide features are observed in avail-

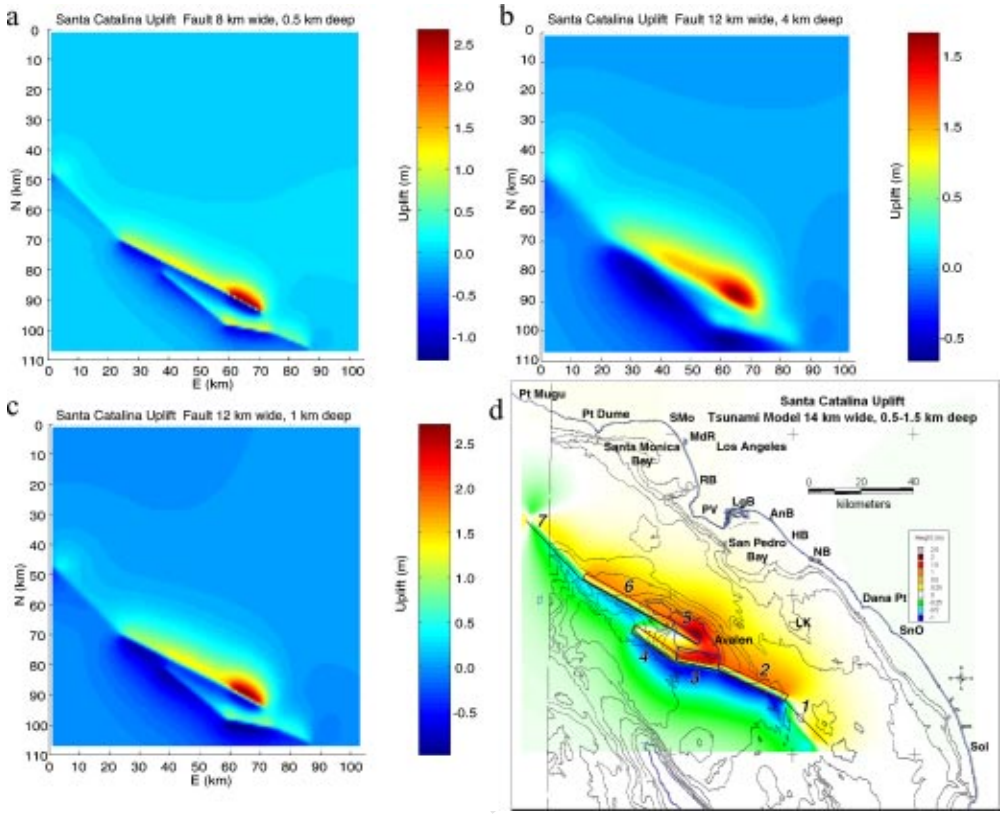

Figure 4. Elastic dislocation models of the surface uplift predicted using seven planar, rectangular, segments along the Catalina Fault showing the variation due to fault width and subsurface depth. (a) Narrow fault (8 km) and shallow depth (0.5 km) produces narrow seafloor uplift and initial wave. (b) Wide fault (12 km) and greater depth (4 km) produces uplift that is too broad and smoothed. (c) Wide fault (12 km) but shallow depth (1 km) produces better fit to island. (d) Wider fault (14 km) and moderate to shallow depth (0.5–1.5 km) produces uplift that matches island morphology. **SMo** Santa Monica, **MdR** Marina del Rey, **RB** Redondo Beach, **PV** Palos Verdes Hills, **LgB** Long Beach, **AnB** Anaheim Bay, **HB** Huntington Beach, **NB** Newport Beach, **SnO** San Onofre, **LK** Lasuen Knoll.

able high-resolution bathymetry (C. Goldfinger, pers. comm., 2003). Consequently, matching the shape of the uplift through elastic modeling of the coseismic deformation, properly scaled to represent realistic earthquake displacements for the length and area of fault rupture, should provide an excellent calibration of our source model.

REFINING THE SOURCE

We use an elastic dislocation model based on Okada's (1985) formulas for surface displacement due to shear and tensile faults in a homogeneous, elastic, half space. To test alternative fault rupture models for tsunami generation, the Coulomb program (King

Table 2. Major fault segments for Santa Catalina uplift tsunami models (M_W=7.6 source)

Segment	Slip[1] (m)	Length (km)	Width (km)	Strike (degrees)	Dip (degrees)	Slip Angle[2] (degrees)	Depth[3] (km)
#1	4.0	21.9	14.0	313	89	172.9	0.5
#2	5.0	28.2	14.0	293	85	143.1	1.0
#3	4.8	16.1	14.9	277	70	123.7	1.0
#4	3.6	20.2	14.0	303	80	146.3	1.0
#5	6.4	8.1	14.0	300	80	149.0	1.5
#6	4.5	40.2	14.0	297	80	153.4	1.0
#7	4.1	29.7	14.0	315	89	166.0	0.5

[1] Slip for full seven-segment fault rupture (case 1)
[2] Rake of slip vector measured from horizontal direction, pure right-slip =180 degrees.
[3] Depth to top of fault plane below ground surface (top of elastic half-space).

et al. 1994, Toda et al. 1998) was used to compute vertical displacement at the surface to compare with observed uplift patterns. This allowed quick computation of numerous candidate source models so that we could more effectively define our final tsunami earthquake source.

Preliminary trials with the elastic dislocation modeling showed that a reasonable fit to the mapped faulting and morphology of the uplift could be achieved with seven fault segments (Figure 3; Table 2). The geographic location, strike, and length of each fault segment were derived from existing fault maps and available seismic reflection profiles (Vedder et al. 1974, 1979, 1986). White (1991) identified a major northwest-trending strike-slip fault cutting the southwest side of the island based on interpretations of satellite imagery and field studies. Shaded relief maps of the digital elevation data for Santa Catalina Island show deflected canyons along the trace of this previously unrecognized fault (Figure 3). The seven fault segments comprise two major fault sections–one along the NW part of the uplift and the second along the SW flank of the uplift. These sections form a 90-km-long restraining bend with a 7.5-km to 10-km releasing (right) overlapping fault step-over. The end-to-end fault length modeled is about 140 km. The restraining bend segments trend 18–36 degrees obliquely to the west of the larger right-slip fault system as defined by the Santa Cruz–Catalina Ridge and the San Diego Trough fault zones. The vertical strike-slip fault segments in our Santa Catalina Island uplift model have slightly more west-trending strikes than the San Diego Trough, thus we include a small component of reverse-slip to account for uplift on the ends of the island platform (Table 2).

Fault dip and down-dip width are poorly constrained for many offshore faults including those along the Catalina Escarpment. Recognizing the overall strike-slip character of the San Diego Trough–Catalina/Santa Cruz–Catalina Ridge fault zones, near vertical fault dips are expected. Hence, fault segments #1 and #7 are assigned vertical dip, as observed for segment #7, which follows the 1981 earthquake (Corbett 1984). Seismic reflection profiles across the fault zone at the northwest and southeast ends of the Santa

Catalina Island uplift show vertical or very steep fault dips (Vedder et al. 1974, 1986; ten Brink et al. 2000). The straight trace of the shallow faulting, mapped from closely spaced seismic profiles and the seafloor escarpment, attest to steep fault dip. Where the fault bends toward the west, we infer that the dip shallows slightly and assign northeast dips of 70 and 80 degrees. The shallowest dip lies along the most west-trending segment (#3). The proposed dips of the restraining bend fault segments are consistent with those inferred for the Palos Verdes Fault (70 degrees southwest) beneath the Palos Verdes Hills (Ward and Valensise 1994) and observed for the 1989 Loma Prieta earthquake (60 degrees northeast, Marshall et al. 1991).

Down-dip width and depth-to-the-top of fault rupture were variables tested by elastic dislocation modeling. If the fault width is too small or the fault rupture is too shallow, the predicted uplift pattern is too narrow compared to the observed seafloor/island morphology (Figures 4a and c). If the top of fault rupture is set too deep, then the predicted uplift pattern is too broad and smoothed (Figure 4b). Our best-fitting model uses a down-dip fault width of 14 km and top of faulting varying along strike from depths of 0.5 km to 1.5 km (Figure 4d, Table 2). Thus we predict that brittle faulting (elastic deformation) occurs to depths of 16 km in the vicinity of the Santa Catalina Island restraining bend. This is somewhat deeper than the typical 8-km to 12-km focal depths of strike-slip earthquakes in California (Sibson 1982), although depths of 15 km have been reported in the San Diego area (Magistrale 1993). Thrust and reverse faulting earthquakes are believed to initiate at greater depths. Lee et al. (1979) and Hauksson et al. (1995) report up to 20 km for the Transverse Ranges, while Marshall et al. (1991) report up to 18 km. Furthermore, the Los Angeles Regional Seismic Experiment (LARSE) data at the south end of Santa Catalina Island suggest that a subvertical fault extends beyond 8–10 km depth (ten Brink et al. 2000).

A prominent releasing step-over within a transpressional fault section, along a restraining bend, appears common in southern California (Legg et al. 1999). For example, near San Bernardino, a prominent releasing step-over occurs where the South Branch San Andreas Fault steps to the right (northeast) from the Banning Fault near the San Bernardino Mountains to the Cajon Pass section of the San Andreas Fault (Figure 1; Morton and Matti 1993). Interaction between the San Jacinto and San Andreas faults at Cajon Pass further complicates the seismotectonics in another transtensional zone along the San Andreas Big Bend (Seeber and Armbruster 1995).

The same fault pattern and fault interaction appears to be replicated where the offshore San Clemente Fault merges with the Catalina Fault at the northwest end of the island uplift (Figure 1). The geometry and scale of the Santa Catalina Island restraining bend, with the releasing step-over near the middle and the fault interaction at the northwest end, is remarkably similar to the San Bernardino Mountains segment of the San Andreas Fault where large earthquakes ($M_W \geq 7.3$) are expected to strike (WGCEP 1995).

The last parameters to be conjectured and set in the elastic dislocation model for the large Santa Catalina Island restraining bend earthquake are the displacements on each fault segment. For a total fault rupture length of about 140 km, empirical relations of magnitude versus fault rupture length suggest earthquake magnitudes (M_W) of about

7.4–7.6 (Wells and Coppersmith 1994). Recent large strike-slip earthquakes in southern California and Turkey involved surface rupture lengths exceeding 70 km (M_W=7.3) for Landers (Wald and Heaton 1994) and about 145 km (M_W=7.4) for Izmit, Turkey (Barka et al. 2002). Maximum displacements estimated from modeling the strong ground motion for these earthquakes vary from about 7 m for Landers (Wald and Heaton 1994) to 5.2 m for Izmit, where a tsunami was generated (Barka et al. 2002, EERI 2000). Vertical displacements from the 1989 Loma Prieta earthquake (M_W=6.9, about 40 km rupture length) were comparable to the lateral displacements, about 1.3 m (Marshall et al. 1991). We model 6.4 m of dextral oblique-reverse slip, which results in about 5.5 m right-slip and 3.3 m reverse-slip.

TSUNAMI MODELING

The tsunami modeling process can be divided into three parts: generation, propagation, and runup (Liu et al. 1991). The generation phase includes the formation of an initial disturbance on the ocean surface due to a coseismic deformation of the sea floor. The latter defines the initial condition for the long wave propagation. The deformation on the sea floor is modeled using Okada's (1985) formulas for surface deformation as described earlier. The seafloor deformation field predicted by the elastic dislocation model (Figure 4d) is translated directly to the water surface and used as an initial condition for the propagation and runup phases.

For tsunami propagation and runup, the model known by the acronym "MOST" (**M**ethod **O**f **S**plitting **T**sunami) (Titov and Synolakis 1995, Titov and Gonzalez 1997) was employed. It is the model used by NOAA. MOST uses the fully nonlinear, depth averaged, shallow-water wave equations in characteristic form to simulate the propagation of long waves over an arbitrary bathymetry. For runup, the model uses a moving boundary algorithm (Titov and Synolakis 1995, 1998) that tracks the evolving shoreline.

For this study, 300-m and 150-m bathymetry and topography grids were used to evaluate each of the seven fault rupture scenarios. The initial condition—the coseismic sea floor displacement—was located consistent with geophysical data and translated to the bathymetric and topographic grid. The initial surface displacement was modeled using the seismic parameters for the seven-segment fault model as shown in Table 2. A model time step of 1 sec was used for the 150-m bathymetry grid and 2 sec for the 300-m bathymetry grid.

ANALYSIS AND DISCUSSION

Figure 5 shows the location of the initial surface displacement and the computed runup along the south-facing and west-facing shorelines for the full seven-segment fault rupture source. Runup values are highest along the San Pedro Bay and Santa Monica Bay coasts with runup heights exceeding 2 m in the vicinity of the Los Angeles and Long Beach harbors. Concentrations of higher runup occur in the vicinity of Marina del Rey, Redondo Beach, the Los Angeles and Long Beach harbor area, and the Newport Beach area. Runup heights exceed 1 m for most of the coast between Santa Monica and Dana Point.

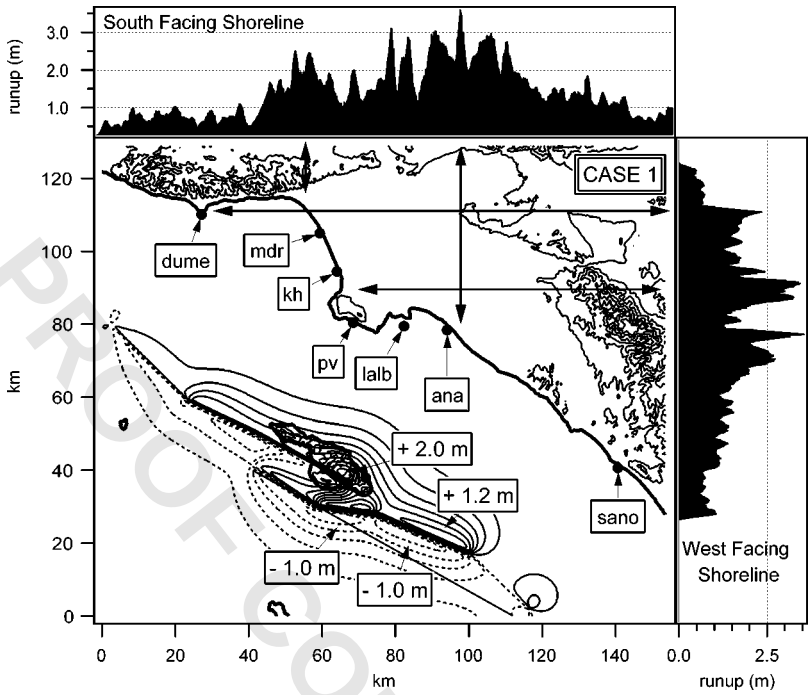

Figure 5. Map showing initial wave height for the full seven-segment Catalina Fault model with graphs of runup along the south-facing and west-facing shorelines. Wave gauge locations are plotted and parameters are listed in Table 3.

Synthetic wave-gauge records are shown for locations along the coast (Table 3, Figures 5 and 6). The wave gauge records show water surface fluctuations that vary from 1–2 m, peak-to-peak, that begin with a leading sea surface rise about 10–18 minutes after the wave was generated. The initial water motion takes from 5–10 minutes to fully

Table 3. Synthetic wave gauge parameters (see Figure 5 for locations)

Name	Symbol	Water Depth (m)
Point Dume	dume	19.2
Marina del Rey	mdr	9.8
King Harbor	kh	12.1
Palos Verdes	pv	23.8
LA/LB Harbor	lalb	9.8
Anaheim Bay	ana	10.3
San Onofre	sano	10.3
Avalon	ava	57.8

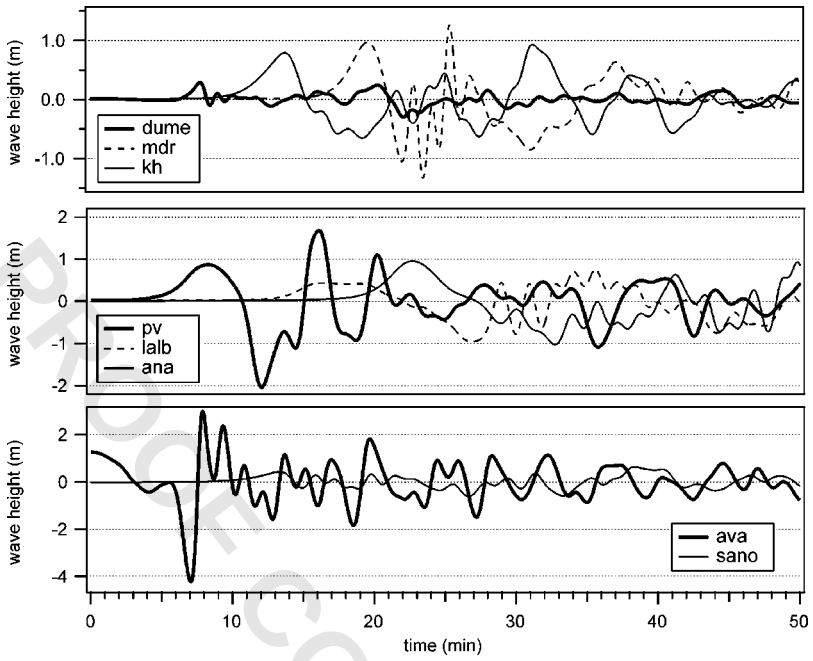

Figure 6. Wave gauge records for the full seven-segment Catalina Fault (M_W=7.6) earthquake (Case 1). Note that the Avalon record starts above zero because the gauge is in the zone of tectonic uplift.

develop and the wave motions persist for more than 50 minutes, after which time the simulation was terminated. Based on the animations produced from the models, the primary wavefront and major refracted wave energy have reached the most distant coastal locations by this time, and as many as three reflected wave oscillations occur. Such long-period oscillations have the potential to generate substantial currents in the narrow openings of harbors—a phenomenon observed in other tsunamis (Borrero et al. 1995). Although the entrance to the Los Angeles and Long Beach harbors are south and east facing, refraction of the waves appears to focus the tsunami energy in this area. More detailed studies are needed, however, to accurately assess the impact of this tsunami source on the Los Angeles and Long Beach harbors and the marine facilities located therein.

Wave periods are generally shorter, about 3–5 minutes for wave gauges along open coast areas with narrow shelves and steep submarine escarpments like Point Dume, Palos Verdes, San Onofre, and Avalon. The large short-period initial wave heights at Palos Verdes and Avalon probably result from amplification of the leading tsunami wave front as it moves up the steep submarine escarpment and crosses the narrow shelf. Marina del Rey, King Harbor, and the Los Angeles/Long Beach harbor gauges show a similar high-amplitude initial wave, at somewhat longer period. These sites also show a second large wave arriving 15–20 minutes after the first large wave. The second-wave runup exceeds

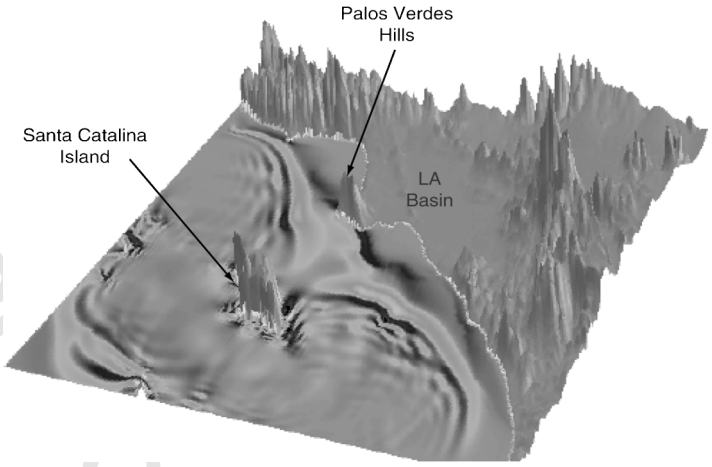

Figure 7. Time step in the MOST tsunami propagation simulation showing the two principal wave fronts generated from the northwest and southeast ends of the submerged Santa Catalina Island platform. Topography has a large vertical exaggeration.

the first for both King Harbor and the Los Angeles/Long Beach harbor gauges, but is slightly smaller for Marina del Rey. A second set of larger waves also arrives at Palos Verdes, but with a longer delay, about 25–30 minutes after the initial wave set, and with about one-third the amplitude of the biggest peak in the first set. Note that the biggest wave is the second wave at Palos Verdes, arriving about 5–10 minutes after the initial wave.

The tsunami generated by the fault model used in this study actually consists of two somewhat separate wave fronts radiating from the northwest and southeast ends of the submerged island uplift (Figure 7). The tsunami separates into these two wave fronts because the highest point of uplift is sub-aerial, occurring near the middle of the island and does not contribute directly to tsunami generation (Figure 4d). As the two wave fronts propagate toward the coast, their interaction forms areas of constructive and destructive interference with local amplification and de-amplification. Constructive interference occurs most strongly at the southern tip of the Palos Verdes peninsula near San Pedro. Changing bathymetry modifies this interaction and creates larger amplifications to the east from the Los Angeles and Long Beach harbors to Anaheim Bay and Newport Beach. Wave refraction further enhances the runup at Marina del Rey and Anaheim Bay as westward-projecting shelf areas form a wave-guide and a gently concave coastline acts to funnel the wave energy.

In Anaheim Bay the first wave arrival occurs 10–15 minutes after the wave arrival at Palos Verdes or Point Dume. Later arrivals at some major coastal harbor facilities could allow for more effective warnings than currently available. For example, wave gauges placed at strategic places along the coast where distant or offshore tsunami would strike first could provide warnings to the port areas located across the relatively broad shelf

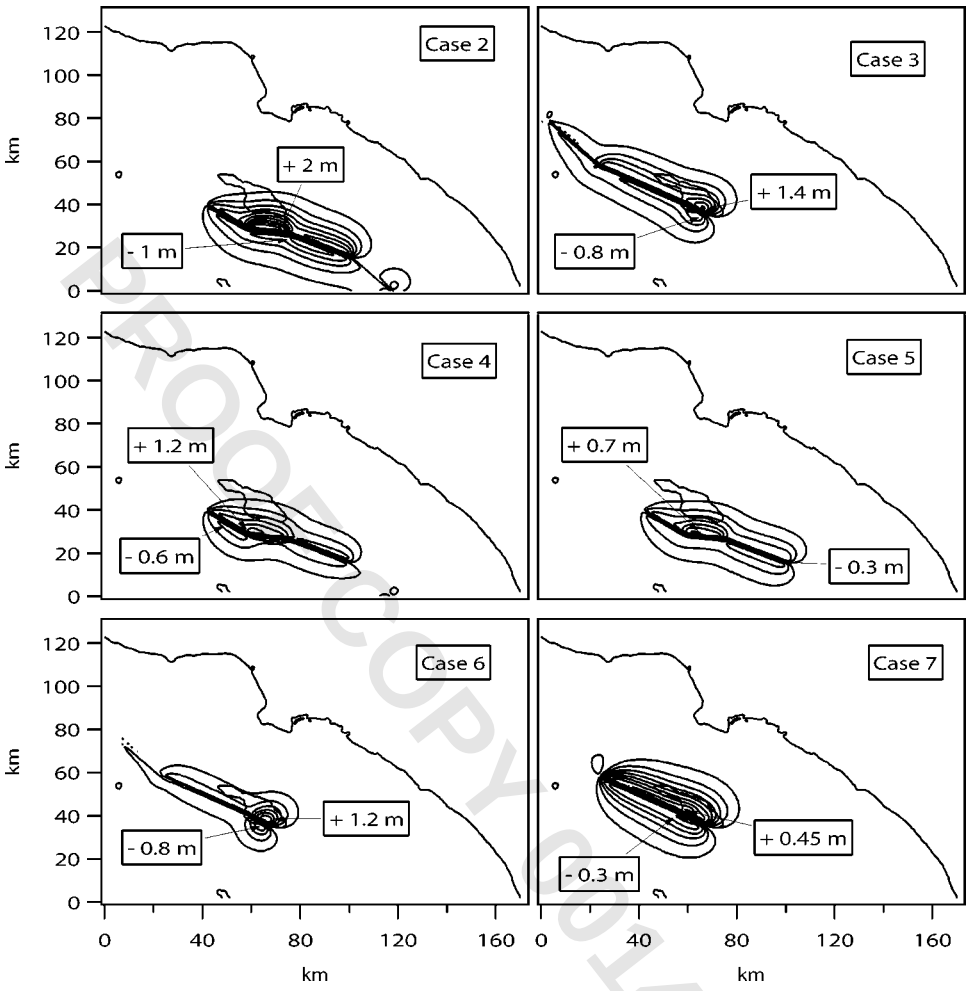

Figure 8. Maps of the initial wave height conditions for the six additional Catalina Fault tsunami scenarios (Table 4).

areas where tsunamis slow down. Deep water gauges as installed by NOAA in the North Pacific (Bernard 2001), but located closer to the active Borderland faults, could provide even more advance warning.

SOURCE VARIABILITY

A single scenario fails to account for the highly variable nature of earthquake and tsunami phenomena. Additional earthquake source models were used to assess the variability in tsunami runup due to large earthquakes on the Catalina Fault. For the present study, six sub-events, comprised of one or more fault segments derived from the full seven-segment model were used (Figure 8, Table 4). These seven scenarios provide a representative measure of the range of runup that may be expected from large earth-

Table 4. Earthquake scenarios for tsunami generation along Santa Catalina uplift

Segments*	Length (km)	Fault Area (km^2)	Max. Slip (m)	Ave. Slip (m)	Magnitude (M_W)	Max. Uplift (m)	Recurrence** (yrs)
1–7	165#	2317	6.4	4.46	7.63	2.17	4,500
1–4	86.5	1225	5.0	4.39	7.44	2.17	4,400
5–7	78.0	1092	6.4	4.54	7.41	1.43	4,500
1–4	86.5	1225	3.6	2.61	7.29	1.30	2,600
2–4	64.6	918.2	3.6	1.50	7.04	0.71	1,500
5–7	78.0	1092	6.4	2.61	7.25	1.39	2,600
5–6	48.3	676.4	2.0	1.92	7.02	0.46	1,900

* See Table 2 for segment parameters; #Includes 25-km overlap of two fault sections.
** Recurrence time (approximate upper bound) assumes 1 mm/yr average slip rate.

quakes on the Catalina fault zone. Furthermore, because these sub-events span the different submarine segments of the Catalina fault zone on both ends of the island, the effects of wave interaction in amplifying runup along the adjacent coast may be distinguished from the effects of source location.

A characteristic earthquake model may be appropriate for the Catalina fault zone, however, available data are inadequate to test it. It is likely that there are many different large "characteristic" earthquake events that combine through geologic time to produce the uplift of the island platform. The six sub-events (Figure 8, Table 4) provide a suite of events that represent the magnitude range ($M_W = 7.0–7.6$) of events large enough to produce potentially destructive local tsunamis, yet are scaled appropriately to reproduce the shape of the island platform morphology. The slip parameters used for each model were scaled down for the shorter fault rupture lengths associated with the smaller sub-events, and are consistent with empirical maximum slip and average slip values versus fault rupture length and magnitude observed in historic earthquakes (Wells and Coppersmith 1994).

It is uncertain whether large strike-slip earthquakes, with some areas of oblique-slip, can rupture completely through major restraining bends. Sibson (1985) proposed that large earthquakes may initiate or terminate at releasing step-overs within major fault zones. Historical earthquakes such as the 1857 Fort Tejon earthquake on the San Andreas Fault appear to have terminated at a significant releasing step-over in the Cajon Pass area. Our model includes a similar releasing step-over within the Santa Catalina Island restraining bend. Paleoseismic evidence suggests, however, that some great ($M_W > 7.5$) earthquakes on the southern San Andreas fault zone may break completely through the Cajon Pass and San Bernardino Mountains segment to the Salton Sea along the Coachella Valley segment (Sieh et al. 1989). Our tsunami modeling considers both types of scenario.

Coastal runup produced by the seven different earthquake scenario tsunamis shows patterns consistent with source geometry, tectonic uplift, and wave refraction due to irregular bathymetry and coastal configuration (Figures 9 and 10). The scenarios involving

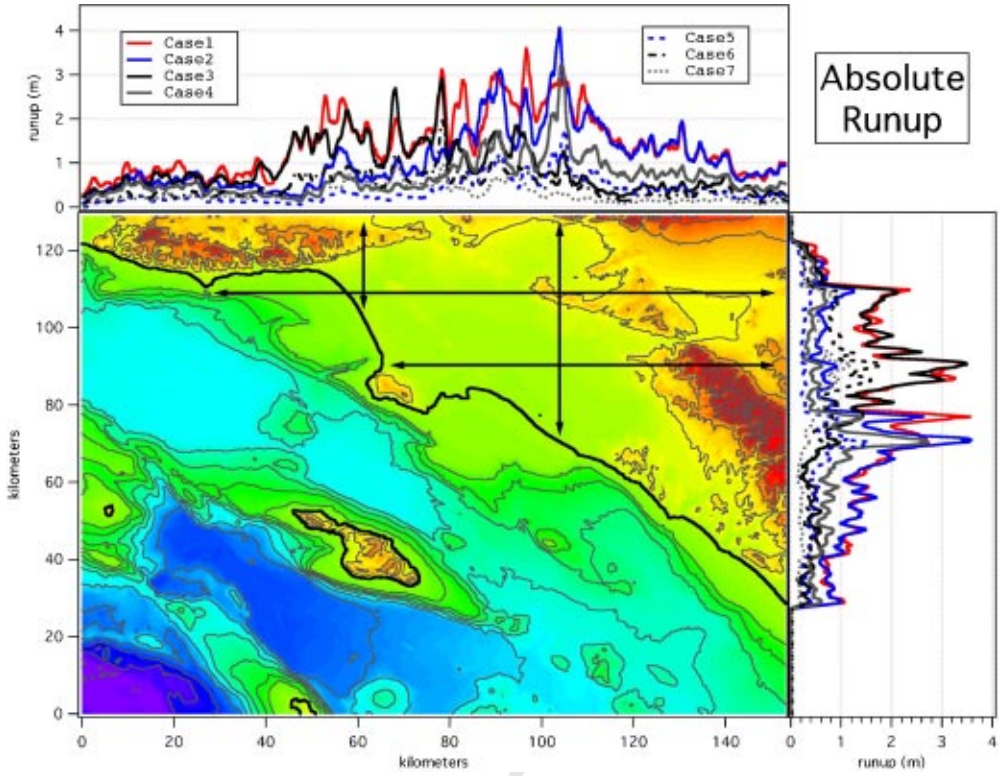

Figure 9. Map showing maximum runup for each of the seven Catalina Fault tsunamigenic earthquake scenarios modeled in this study (fault parameters in Table 4).

rupture of the northwestern fault segments (cases 3, 6, 7) tend to produce higher runup in Santa Monica Bay and those involving rupture of the southeastern fault segments (cases 2, 4, 5) produce higher runup in San Pedro Bay and along the Orange County coast. Figures 7 and 9 suggest that constructive interference between the two separate wavefronts produced by the full seven-segment rupture amplifies the wave heights at the coast in this area. Coastal runup for the other four earthquake scenarios produce similar patterns to those of the northeast or southwest sections at reduced amplitudes commensurate with the smaller earthquake magnitude and vertical displacements (Figure 9). In general, maximum subevent runup values along the coast are roughly one-half the values for the largest earthquake scenarios.

To separate the effects of earthquake magnitude from tsunami wave refraction among different scenarios, computed runup was normalized by the maximum uplift for each scenario (Figure 10). The overall shape of the runup plots are similar for the absolute runup and normalized runup, with peaks located at the harbor areas described above, implying wave refraction effects. Indeed, the tsunami from the 1960 Chilean (M_W=9.5) earthquake was strongly amplified in the Marina del Rey area where the tide gauge was clipped for two hours with measurements in excess of 3 m peak-to-peak. Os-

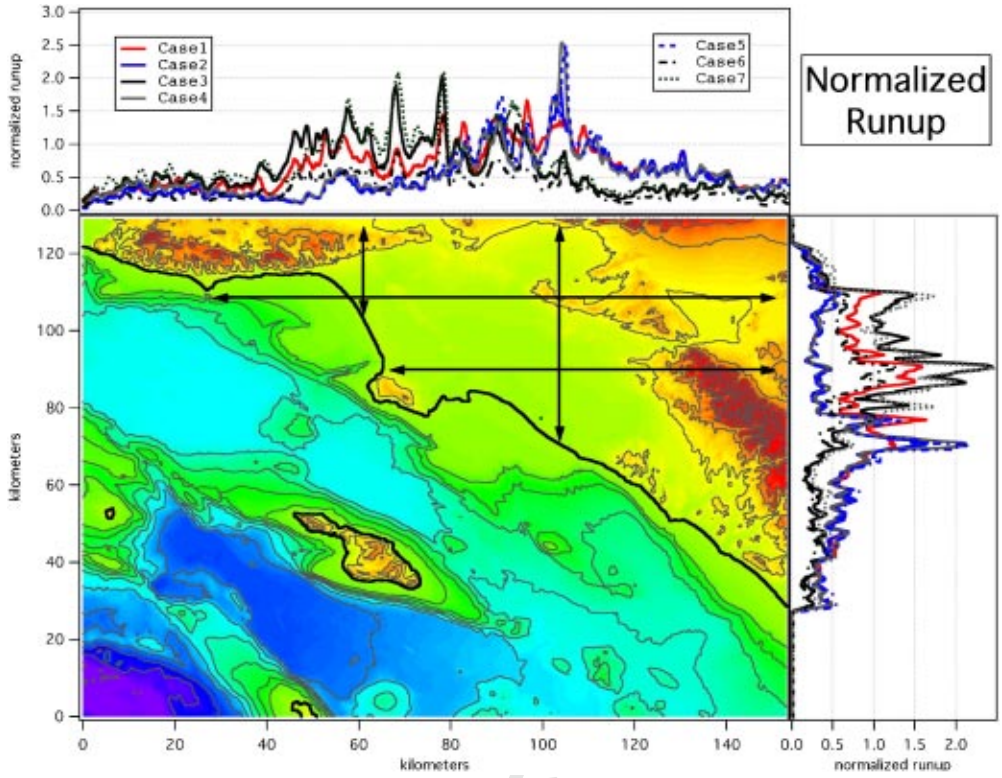

Figure 10. Map showing maximum runup normalized to the maximum seafloor/island uplift for each of the seven Catalina Fault tsunamigenic earthquake scenarios modeled in this study (fault parameters in Table 4).

cillations persisted with high amplitudes (>1 m) for more than ten hours (Lander et al. 1993). Wave heights are also amplified around the northwestern end of the Palos Verdes peninsula, possibly due to similar refraction effects but also because of less attenuation due to the shorter distance from the fault rupture source.

Previous tsunami hazard studies along the southern California (Houston 1980, McCulloch 1985, Borrero 2002) show similar patterns of amplification in Santa Monica Bay and San Pedro Bay with less amplification at the Palos Verdes peninsula. The pre-2001 studies were based on distant tsunami sources, from Alaska or South America, so that the geometrical spreading attenuation effects are reduced for the long period waves once they reach southern California. Normalized runup plots show that the maximum amplification of tsunami wave height along the coast is less than 250 percent (Figure 10; Table 4). The runup computed with the MOST program is for a smoothed coastline and computational grid resolution as fine as 150 m so that local amplification at higher spatial frequencies is smoothed out. In general, coastal runup lies between 50 and 150 percent of the maximum tectonic uplift due to the fault rupture. Consequently, if local high-

slip patches occur with greater seafloor uplift than predicted from the simple elastic dislocation model, adjacent coastal areas may experience higher runup.

Our models predict coastal runup ranging from 0.5 to 3.6 m for offshore earthquakes with moment magnitudes between 7.0 and 7.6. Conservatively assuming a factor of two uncertainty, for the reasons discussed above, local tsunamis from earthquakes along the Catalina fault system may produce coastal runup from 1 to 7 m in elevation. A maximum runup of 7.3 m was observed from the 1994 Mindoro, Philippines, earthquake (magnitude 7.1) strike-slip earthquake (Daag et al. 1995, Imamura et al. 1995). If the variability can reach a factor of 6.5 as found by Geist (2002) for stochastic simulations of Central Mexico subduction earthquakes, then maximum runup from large local southern California tsunamis may be significantly larger. The difficulty arises because we cannot yet a priori predict the complex slip distribution in a large earthquake, and the maximum runup and wave height is directly proportional to the maximum seafloor uplift. As Geist (2002) shows, and as observed in the 2001 Camana, Peru, tsunami (Okal et al. 2002), local high-slip patches are responsible for the maximum runup.

LIMITATIONS OF THE MODEL

Because the Catalina fault system is predominately strike-slip in character, the maximum seafloor uplift is less than other southern California fault systems where thrust or reverse faulting predominates. Roughly equal partitioning between strike-slip and dip-slip was observed in the 1989 Loma Prieta earthquake within the predominately right-slip San Andreas fault system (Marshall et al. 1991). Thus we might expect similar partitioning along the Catalina fault system. As observed in the Philippines, however, large strike-slip earthquakes may still produce destructive tsunamis.

Despite our attempts to realistically model the earthquake source for tsunami generation, the models developed remain quite simple compared to actual observed earthquake fault rupture parameters (Sieh et al. 1993, Wald and Heaton 1994). Our simple models ignore the dynamic aspects of the fault rupture process and use only the static displacement. Our simple models involve planar rectangular fault segments with uniform slip for each segment, whereas the distribution of slip within real earthquakes is more complex with local areas of high slip with irregular geometry. Often there may be several active faults involved in one large earthquake, with complex distributions of slip on each segment. Variability of the slip distribution from one characteristic earthquake to the next on a particular fault is also observed in real earthquakes such as the 1940 Imperial Valley and 1979 El Centro earthquakes on the Imperial Fault (Sharp 1982, USGS 1982). Since the elastic models smooth out the details of fault rupture at the surface, we conjecture that our simple models provide a first order representation of real earthquake variability with regard to the scales involved in local tsunami generation.

One area of concern is that the elastic dislocation model produces smaller vertical displacements than the maximum fault slip on the modeled fault surfaces. This result may be reasonable for buried fault sources where no surface rupture occurs (e.g., 1989 Loma Prieta earthquake, Marshall et al. 1991). However, where surface or seafloor fault rupture occurs, the maximum surface displacement is comparable to the maximum subsurface displacement values derived through seismological observations (Wald and

Heaton 1994, Treiman et al. 2002). Seafloor fault scarps of 1–3 m height, likely resultant from prehistoric large earthquakes, have been observed on major faults offshore southern California (Goldfinger et al. 2000). Because we typically observe only about one-half the maximum subsurface slip value as surface displacement in the elastic dislocation model, we suspect that our estimates of seafloor uplift and initial tsunami wave height may be too low by a factor of two. This proposition is supported by observations of recent tsunamis around the world where the measured maximum runup values also tend to be about twice the predicted values from elastic dislocation models of tectonic faulting based on seismological observations (cf., Geist 2002, Borrero et al. 2003).

TSUNAMI RECURRENCE AND STATISTICS

The Santa Catalina Island uplift is one of the largest elevated structures in the Inner Borderland of southern California, south of the Transverse Ranges. Therefore, the Catalina fault system may represent the most significant local tsunami source. A conservative approach to tsunami hazard assessment is to consider the tsunami runup modeled for the Santa Catalina Island uplift and Catalina fault system, and estimate recurrence times based on overall slip rates for offshore fault systems in southern California.

No published estimates of the slip rate for the Catalina fault system are available at this time. Based on the well-defined character of the Catalina and San Diego Trough fault zones, the slip rate is likely to be similar to that of other well-defined fault zones in southern California. The Palos Verdes and Newport-Inglewood-Rose Canyon fault zones have slip rates measured at 1–3 mm/yr (Fischer and Mills 1991, Lindvall and Rockwell 1995, McNeilan et al. 1996). Preliminary estimates of slip rates for the San Clemente fault zone south of San Clemente Island are 4–7 mm/yr (Legg 1985). Geodetic estimates of present-day tectonic plate motions suggest that as much as 20 percent of the Pacific–North America relative motion occurs offshore southern California—roughly 10 mm/yr (Demets and Dixon 1999, Sella et al. 2002).

Only a small number of potential earthquake-generated tsunamis are modeled in this study, and so the full range of potential scenarios for local southern California tsunamis may be poorly represented. Geist (2002) shows that the complexity in real earthquakes may produce variability in tsunami amplitudes of a factor of 2.5 or more for an earthquake of constant M_W and location. The variability from our seven scenarios approaches a factor of 5.0 for an earthquake magnitude range of about 0.6, while tsunami amplitudes vary by a factor of 1.8 for a specific magnitude (Table 4). Including the uncertainties in the elastic dislocation models, our results provide a reasonable first-order hazard assessment for local tsunamis in southern California.

Two methods based on average displacement rates are used to estimate the occurrence frequency of the large earthquakes modeled and the associated local tsunami hazard. The first method, commonly used in paleoseismic analyses, assumes a characteristic earthquake model and divides the average event slip by the average fault slip rate to derive a recurrence interval. The second method recognizes that natural complexity and strain partitioning in earthquake fault rupture results in some earthquakes with mostly strike-slip mechanisms (1906 San Francisco) and others with significant dip-slip mechanisms (1989 Loma Prieta). Thus a more accurate estimate of recurrence times for locally

generated tsunamis may be provided by dividing the maximum uplift for the earthquake scenario by the average rate of uplift of Santa Catalina Island. Similar analyses have been made using uplift of the Palos Verdes Hills to estimate the slip rate on the Palos Verdes fault zone (Ward and Valensise 1994) and of the Santa Cruz Mountains (Valensise and Ward 1990) for the recurrence of Loma Prieta–type earthquakes.

Using a simple assumed slip rate of 1 mm/yr for right-slip along the Catalina fault system, the recurrence time for large ($M_W \geq 7$) earthquakes in the Santa Catalina Island uplift area would be about 1,500–4,500 years (Table 4). If the maximum rate of right-slip for the offshore region is used, about 10 mm/yr, then the recurrence time is reduced accordingly to 150–450 years. No offshore earthquakes of this magnitude have been recorded in the brief history of the southern California region. Large earthquakes with possible offshore epicenters are reported in the Oceanside area on 22 November 1800 and in the Santa Barbara Channel area on 21 December 1812. Farther north, a large earthquake struck offshore Point Arguello on 4 November 1927. Thus recurrence times of a few hundred years for $M_W \sim 7$ earthquakes offshore southern California may be a reasonable first-order estimate. Recurrence times of several hundred to a few thousand years for $M_W > 7$ earthquakes on the Catalina Fault with significant seafloor uplift and local tsunami generation seem appropriate.

The total structural relief across the Catalina fault system is approximately 2,250 m, measured from the 650-m elevation for Mt. Orizaba to the 300-m basin fill below the 1,300-m deep escarpment (Vedder 1987). In middle Miocene time, when most of the volcanic rocks on the Santa Catalina Island were emplaced, the area was at or above sea level (Vedder et al. 1979). It then subsided rapidly at the end of Miocene into early Pliocene time reaching abyssal depths in some areas (~2,000 m). The uplift of the Santa Catalina Island platform to its present elevation occurred since early Pliocene time, within the last 3–6 Myrs. The Palos Verdes Hills uplift occurred in this same time period (Nardin and Henyey 1978), whereas the Signal Hill uplift occurred more recently, during the last 200 ka (Ponti and Lajoie 1992).

Using the available geological data, a minimum average rate of tectonic uplift for Santa Catalina Island is 0.375–0.75 mm/yr. Measured rates of tectonic uplift in the southern California coastal area range from 0.1–0.4 mm/yr for elevated Pleistocene marine terraces on the coast and offshore islands south of the WTR (Lajoie et al. 1992). Higher rates (~3 mm/yr) are measured near Ventura and Cape Mendocino where active faulting has greater vertical slip. Assuming that uplift of Santa Catalina Island occurred tectonically through large earthquakes as modeled above, the estimated recurrence times for $M_W = 7.0–7.6$ events on the Catalina fault system is about 600–6,000 years. Based upon paleoseismic studies (Rockwell et al. 2000, Tucker and Dolan 2001), other large seismogenic faults in the Los Angeles and southern California area have similar recurrence times.

LANDSLIDE VS. EARTHQUAKE TSUNAMI SOURCES

The runup values predicted in this study ignore the possibility of large submarine landslides being triggered by the earthquake. Larger runup associated with large submarine landslides offshore southern California has been estimated in recent studies (Bor-

rero et al. 2001, Borrero 2002), but this study focuses on the tectonic sources only. The schist basement rock of Santa Catalina and adjacent offshore areas is prone to landsliding (Vedder et al. 1979) and large-scale basement-involved landslides have been mapped in the southern California offshore area (Legg and Kamerling 2003). A large earthquake on the Catalina fault system could generate a large landslide and generate additional tsunami wave energy. Further research is needed to examine this possibility and estimate the wave height and runup expected from realistic submarine landslide sources around the island.

Numerous submarine landslides have been mapped in the California Continental Borderland (Greene and Kennedy 1987; Field and Edwards 1980, 1993; Legg and Kamerling 2003). Even though submarine landslides may be triggered by large earthquakes offshore, or on coastal or onshore fault systems like the San Andreas, such as occurred in Monterey Bay during the 1989 Loma Prieta earthquake (Schwing et al. 1990, McCarthy et al. 1993), large possibly catastrophic submarine landslides appear to be relatively rare offshore southern California. For example, the large basement-involved landslide described by Legg and Kamerling (2003) appears to be more than 100 ka, and the large San Pedro Canyon submarine landslide is about 7,500 years old (Fisher 2002). Large earthquakes, with $M_W \geq 7$ involving slip of 1–6 m would have recurrence times of a few hundred to a few thousand years, substantially shorter than the suspected frequency of large submarine landslides in the borderland. Consequently, the first-order driving force for local tsunamis offshore southern California is expected to be tectonic deformation from large earthquakes.

SUMMARY AND CONCLUSIONS

To evaluate the potential for destructive tsunami generated by local earthquakes offshore southern California, we model the Santa Catalina Island restraining bend with a realistic fault geometry and oblique-reverse earthquake displacement field to match the overall shape of the island block morphology. We successfully reproduce the shape of the Santa Catalina Island platform uplift using a 140-km-long, seven-segment, elastic dislocation fault model with a maximum displacement of 6.4 m. The displacement on each fault segment was adjusted in both right-slip and reverse-slip components to produce the uplift pattern with the amplitudes scaled to realistic values for large earthquakes ($M_W \geq 7$). To estimate the variability of potential earthquakes and seafloor displacement, a suite of six sub-events, $M_W = 7.0–7.4$ (Table 4) were modeled using various combinations of the seven fault segments. Segment displacements were scaled to values appropriate for the fault rupture length and earthquake magnitude. The relative proportions of right-slip and reverse-slip of the seven-segment model were maintained to produce the overall shape of the island uplift.

The vertical displacement produced by each elastic dislocation model was used as a static displacement initial condition for the sea surface representing coseismic generation of a tsunami. Although maximum tectonic uplift varied from about 0.5 to 2.2 m, the initial wave height was reduced because the highest uplift occurs on the sub-aerial part of the island. Maximum subsidence on the footwall block southwest of the Catalina escarpment exceeded 1.3 m. The presence of the island effectively separates the initial sea surface uplift into two northwest-trending wave fronts.

Significant runup was modeled along the southern California coast from Point Mugu to Solana Beach, both at the ends of the model bathymetry grid. Maximum runup exceeds one meter along most of the coast between Santa Monica and Dana Point, with peaks of 1.5 to 4.0 m at Marina del Rey, Redondo Beach, Los Angeles and Long Beach harbors, and the Orange County coast from Seal Beach to Newport Beach. Some of the most severely affected areas correspond to the major harbor areas where marine terminals and boating facilities are located. Experience from historical distant tsunamis such as generated by the 1960 Chilean and 1964 Alaskan earthquakes show that these harbor areas are vulnerable to strong currents that can scour pilings and damage boats (Lander et al. 1993).

Recent observations of tsunami runup following large earthquakes worldwide suggest that runup values predicted from simple elastic dislocation models of tectonic deformation underestimate the observed peak runup values by a factor of two or more. Complex tectonic source models are often necessary to reproduce observed runup values (Takahashi et al. 1995, Piatanesi et al. 1996). Complex interactions between the tsunami wave field and local bathymetry and coastal configuration may create locally severe wave amplification and runup. Consequently, actual coastal runup values from large earthquakes on the Santa Catalina Island restraining bend may exceed 7 m.

Travel time between the earthquake occurrence and arrival of the first waves ranges from about 10 to 20 minutes for the areas most severely affected, i.e., adjacent mainland coast, making official warnings broadcast in sufficient time for evacuation difficult. The strong earthquake will provide the only warning to coastal residents, and concurrent quake-related damage, including potential widespread liquefaction and failures of oversteepened coastal bluffs, may exacerbate evacuation or rescue efforts. Fortunately, large earthquakes on this major offshore fault system appear to be infrequent, with estimated recurrence intervals of several hundred to thousands of years. However, if clustering of events is characteristic of major fault systems offshore southern California, as has been interpreted for several onshore fault systems, the local tsunami hazard may be enhanced during the cluster period. Further study is needed to measure slip rates on the major offshore fault systems and to identify the frequency and magnitude of large prehistoric submarine earthquakes that may have generated potentially destructive local or regional tsunamis. Likewise, direct geological investigations to identify possible prehistoric tsunami deposits along the southern California coast are urgently needed to quantify more accurately offshore threats. Meanwhile, coastal construction including major marine terminals, power plants, and other important coastal facilities should proactively evaluate their local tsunami hazard, structural and human vulnerabilities, and level of exposure to provide more accurate risk assessment and so as to implement effective risk reduction measures.

Last, this study only examined the tectonic deformation from large earthquakes as potential tsunami source. Large-scale submarine landslides represent a serious threat, and the earthquakes we have modeled would very likely trigger widespread slope failures, both sub-aerial landslides along the coastal bluffs and submarine landslides along the steep borderland slopes. The 1994 Papua New Guinea tsunami of landslide origin shows that the near-source landslide-generated tsunami runup may greatly exceed that

from tectonic deformation (Synolakis et al. 2002). A realistic earthquake scenario should consider both tectonic and coseismic landslide sources of local tsunamis.

ACKNOWLEDGMENTS

This paper results from the 2002 EERI/FEMA NEHRP Professional Fellowship to Dr. Legg. Angie Venturato (NOAA) provided updated bathymetry and topography for use in the MOST modeling program. Dr. Shun-Ichi Koshimura provided the elastic dislocation model used in the tsunami simulations. The authors are grateful to Professor Lori Dengler, Dr. Eric Geist, and an anonymous reviewer for their thorough manuscript reviews and comments, which substantially improved the content of this paper.

APPENDIX

Although the hazard to metropolitan southern California posed by locally generated tsunamis has received considerably less study than the hazards posed by onshore earthquakes, several locally generated tsunamis have been reported in the past 200 years. In fact, one of the first large earthquakes to be reported in southern California, the 21 December 1812 Santa Barbara earthquake, appears to have generated a moderate tsunami that affected more than 60 km of the Santa Barbara coast (Toppozada et al. 1981, Lander et al. 1993). Refer to Figure 1 for the locations mentioned below.

THE 21 DECEMBER 1812 SANTA BARBARA EARTHQUAKE

This earthquake caused extensive damage to the Spanish missions of Santa Barbara, Ventura, and La Purisima at Lompoc. Felt intensity reports suggest that the 21 December 1812 Santa Barbara earthquake had a moment magnitude equivalent to 7.2 (Toppozada et al. 1981, Ellsworth, 1990). Toppozada et al. (2002) suggest that the earthquake was located along the San Andreas Fault, whereas the previous studies inferred a location within the Santa Barbara Channel area.

Historical sources report unusual ocean activity and high waves after the 21 December 1812 tremor (Toppozada et al. 1981). Runup from this event is believed to have been up to 4 m at El Refugio (40 km west of Santa Barbara), and around 2 m in Santa Barbara and Ventura. Contemporary eyewitness accounts describe a leading depression wave (Tadepalli and Synolakis 1994), one that recedes first leaving the near-shore area exposed (McCulloch 1985, Lander et al. 1993). Other accounts from survivors describe how residents relocated their settlements further inland after being flooded by unusual waves (Toppozada et al. 1981). An inspection of historical records in Hawaii suggests that this event may have been observed as a 2- to 4-m-high wave in Hilo (Lander et al. 1993). The actual tsunami source may have been a submarine landslide (Lander et al. 1993, Greene and Maher 2000, Borrero et al. 2001), yet if the wave observed in Hawaii was generated by the southern California earthquake a submarine tectonic source in the Santa Barbara Channel region, is more likely. Furthermore, accounts of a ship being damaged by the shock (Lander et al. 1993) are consistent with a submarine earthquake rather than a southern San Andreas earthquake.

THE 27 MAY 1862 SAN DIEGO EARTHQUAKE

A moderate earthquake struck the San Diego area on 27 May 1862, with an estimated local magnitude 6.2 (Legg and Agnew 1979; Toppozada et al. 1981, 2000). Although damage to San Diego buildings was light, the maximum intensity of the main shock (Modified Mercalli, MMI=VII) and frequency of aftershocks kept many residents sleeping outdoors for nearly two weeks (Legg and Agnew 1979). A contemporary report by Andrew Cassidy (Agnew 1979), the tide gauge engineer, noted, "The water of the Bay did not appear to be much agitated notwithstanding the sea run up on the beach between 3 and 4 feet, and immediately returned to its usual level." Unfortunately, he was in the process of repairing the tide gauge pier at the time, so that no tide gauge records are available. It is still uncertain whether the wave was generated by tectonic displacement, landsliding from the bluffs at Point Loma nearby the tide gauge, or a seiche in San Diego Bay.

THE 4 NOVEMBER 1927 LOMPOC EARTHQUAKE

The largest and best observed locally generated tsunami on the California coast was generated by the large (M_S=7.3) 4 November 1927 Point Arguello–Lompoc earthquake northwest of Point Conception (Byerly 1930, Hanks 1979, Satake and Somerville 1992). The causative fault and exact location of this earthquake have been much debated, but is generally thought to be one of the northwest-trending, offshore thrust, or oblique-reverse faults that parallel the coast in this region. The tsunami generated by this event was observed in several locations along the central California coast. A 2-m wave was reported in Surf, while at Port San Luis (see Figure 1) a 2-m leading depression wave was followed by a leading elevation wave of similar height. This event produced a 10-cm tsunami height on a tidal gauge in Hilo, Hawaii (Byerly 1930, Satake and Somerville 1992).

THE 31 AUGUST 1930 SANTA MONICA BAY EARTHQUAKE

A moderate earthquake (M_W~5.2), centered inside Santa Monica Bay, was widely felt across the southern California region (Hauksson and Saldivar 1986, Hauksson 1990). Gutenberg et al. (1932) reported a central area of intensity MMI=V extending from Santa Monica to Pasadena, southward into northern Orange County and northwestward to southern Ventura County. Light to moderate damage to buildings in Los Angeles, Santa Monica, and Venice resulted in maximum intensities of MMI=VII–VIII (Gutenberg et al. 1932). The intensity reportedly diminished radially outwards to very low levels, including Santa Barbara and southern Orange County. The shaking was felt as far as Riverside and Barstow approximately 100 and 150 km to the east of Los Angeles. Lander et al. (1993) describe the event in some detail and suggest a local landslide-generated tsunami, whereas Gutenberg et al. (1932) report no tsunami records on the local tide gauge.

THE 10 MARCH 1933 LONG BEACH EARTHQUAKE

One of the first significant instrumentally recorded earthquakes in southern California was the M_W=6.4 (Hauksson and Gross 1991) Long Beach earthquake, which caused

extensive damage in Long Beach and Compton, California. The earthquake occurred along the Newport-Inglewood fault zone (NIFZ) and was almost purely strike-slip in nature (Hauksson and Gross 1991). The earthquake epicenter was located along the coast at Newport Beach, and the rupture propagated to the northwest for approximately 15 km to the city of Long Beach. An estimated 85 to 120 cm of right-slip occurred at depth along the rupture surface (Hauksson and Gross 1991). No tsunami has yet been directly related to the event (Lander et al. 1993). This event is suggestive of the potential for strong earthquakes in the nearshore region.

THE 1981 SANTA BARBARA ISLAND AND 1986 OCEANSIDE EARTHQUAKES

The Catalina Fault lies between the Santa Cruz–Catalina Ridge Fault and the San Diego Trough Fault, where two moderate earthquakes occurred during the past century (Figure 1). Neither the earthquake of 4 September 1981 (M_W=6.0, M_L=5.3; Corbett 1984; Bent and Helmberger 1991) nor the earthquake of 13 July 1986 (M_S=5.8, M_L =5.3; Hauksson and Jones 1988) generated local tsunamis. Both events had substantial long-period energy release as their surface wave and moment magnitudes exceeded the local Richter magnitude reported in the southern California earthquake catalog. The 1981 earthquake had a strike-slip mechanism (Corbett 1984), whereas the 1986 earthquake had a blind thrust mechanism (Hauksson and Jones 1988, Pacheco and Nabelek 1988). Both earthquakes had rich aftershock sequences, a narrow pattern aligned along the Santa Cruz–Catalina Ridge consistent with the 1981 right-slip mechanism (Corbett 1984), and a broad diffuse cloud of aftershocks located to the northwest of the 1986 main shock (Hauksson and Jones 1988, Astiz and Shearer 2000) consistent with thrust faulting. The 1986 earthquake was located near a small restraining bend at the northwest end of the right-lateral San Diego Trough fault zone (Hauksson and Jones 1988), which lies to the southeast of the Catalina Fault (Figure 1). These events resemble patterns along the San Andreas Fault, where a large strike- slip earthquake ruptured most of the northern San Andreas Fault in 1906, while a smaller blind thrust earthquake in 1989 ruptured within a restraining bend at Loma Prieta. Large earthquakes that rupture the intervening section of the Catalina Fault may have both dip-slip and reverse-slip character, and may therefore generate destructive local tsunamis.

THE 17 OCTOBER 1989 LOMA PRIETA EARTHQUAKE

This earthquake (M_W=6.9) was located approximately 100 km south of San Francisco. It involved a 5-km to 17-km-deep oblique-reverse fault rupture along northwest strike and northeast dip within the Santa Cruz Mountains restraining bend segment of the San Andreas fault zone (Marshall et al. 1991). The event caused extensive shaking damage to several cities in the San Francisco Bay area and a small tsunami in Monterey Bay (Schwing et al. 1990). Like the proposed Catalina Fault scenario, this event occurred along a restraining bend of a strike-slip fault. Furthermore, there is evidence that the tsunami may have had both tectonic and submarine landslide triggers (Schwing et al. 1990, Ma et al. 1991).

REFERENCES

Agnew, D. C., 1979. Tsunami history of San Diego, in *Earthquakes and Other Perils—San Diego Region*, edited by P. L. Abbott and W. J. Elliott, San Diego Association of Geologists guidebook, pp. 117–123.

Astiz, L., and Shearer, P. M., 2000. Earthquake locations in the inner Continental Borderland offshore southern California, *Bull. Seismol. Soc. Am.* **90**, 425–449.

Barka, A., and 21 others, 2002. The surface rupture and slip distribution of the 17 August 1999 Izmit earthquake (M 7.4), North Anatolian Fault, *Bull. Seismol. Soc. Am.* **92**, 43–60.

Bennett, R. A., Rodi, W., and Reilinger, R. E., 1996. Global Positioning System constraints on fault slip rates in southern California and northern Baja, Mexico, *J. Geophys. Res., [Space Phys.]* **101**, 21943–21960.

Bent, A. L., and Helmberger, D. V., 1991. Seismic characteristics of earthquakes along the offshore extension of the Western Transverse Ranges, California, *Bull. Seismol. Soc. Am.* **81**, 399–422.

Bernard, E. N., 2001. The U.S. National Tsunami Hazard Mitigation Program Summary in *Proceedings of the International Tsunami Symposium 2001, NOAA/PMEL, Seattle, WA*, p. 21.

Borrero, J. C., 2002. Tsunami Hazards in Southern California, Ph.D. Thesis, University of Southern California, Los Angeles, CA, 306 pp.

Borrero, J. C., Dolan, J. F., and Synolakis, C. E., 2001. Tsunamis within the eastern Santa Barbara Channel, *Geophys. Res. Lett.* **28**, 643–646.

Borrero, J., Ortiz, M., Titov, V., and Synolakis, C., 1995. Field survey of Mexican tsunami produces new data, unusual photos, *EOS Trans. Am. Geophys. Union* **88**, 87–88.

Borrero, J. C., Saiang, C., Uslu, B., Freckman, J., Gomer, B., Okal, E. A., and Synolakis, C. E., 2003. Field survey and preliminary modeling of the Wewak, Papua New Guinea earthquake and tsunami of 9 September, 2002, *Seismol. Res. Lett.* **74**, 393–405.

Byerly, P., 1930. The California earthquake of November 4, 1927, *Bull. Seismol. Soc. Am.* **20**, 53–66.

Clarke, S. H., Greene, H. G., Kennedy, M. P., and Vedder, J. G., 1987. Geologic map of the inner-southern California continental margin, California Division of Mines and Geology, *California Continental Margin Geologic Map Series*, Area 1 of 7, sheet 1 of 4, scale 1:250,000.

Corbett, E. J., 1984. Seismicity and Crustal Structure Studies of Southern California: Tectonic Implications from Improved Earthquake Locations, Ph.D. dissertation, California Institute of Technology, Pasadena, California, 231 pp.

Crouch, J. K., and Suppe, J., 1993. Late Cenozoic tectonic evolution of the Los Angeles basin and inner California borderland: A model for core complex-like crustal extension, *Geol. Soc. Am. Bull.* **105**, 1415–1434.

Crowell, J. C., 1974. Origin of late Cenozoic basins in southern California, in *Tectonics and Sedimentation*, edited by W. R. Dickinson, Society of Economic Paleontologists and Mineralogists, *Spec. Publ. - Soc. Econ. Paleontol. Mineral.* **22**, 190–204.

Daag, A. S., De los Reyes, P. J., Tubianosa, B. S., Javier, D. V., and Punongbayan, R. S., 1995. Tsunami deposit of the 15 November 1994 Mindoro earthquake, Philippines, *Proceedings, Tsunami Deposits, Geologic Warnings of Future Inundation, University of Washington, Seattle, 22–23 May 1995*, p. 3.

DeMets, C., and Dixon, T. H., 1999. New kinematic models for Pacific-North America motion

from 3 Ma to present, I: Evidence for steady motion and biases in the NUVEL-1A model, *Geophys. Res. Lett.* **26**, 1921–1924.

Earthquake Engineering Research Institute, 2000. 1999 Kocaeli, Turkey, Earthquake Reconnaissance Report, *Earthquake Spectra*, Supplement A to volume 16, Ch. 3: Tsunami Waves in Izmit Bay, pp. 55–62.

Ellsworth, W. L., 1990. Earthquake history, 1769–1989, in *The San Andreas Fault System, California*, edited by R. E. Wallace, *U.S. Geol. Surv. Prof. Pap. 1515*.

Field, M. E., and Edwards, B. D., 1980. Slopes of the southern California borderland: A regime of mass transport, in *Pacific Coast Paleogeography Symposium No. 4*, edited by M. E. Field, A. H. Bouma, I. P. Colburn, R. G. Douglas, and J. C. Ingle, Los Angeles, Pacific Section SEPM, pp. 169–184.

Field, M. E., and Edwards, B. D., 1993. Submarine landslides in a basin and ridge setting, southern California, in *Submarine Landslides: Selected Studies in the U.S. Exclusive Economic Zone*, edited by W. C. Schwab, H. J. Lee, and D. C. Twichell, U.S. Geological Survey Bulletin 2002, 176–183.

Fischer, P. J., and Mills, G. L., 1991. The offshore Newport-Inglewood-Rose Canyon fault zone, California: Structure, segmentation, and tectonics, in *Environmental Perils of the San Diego Region*, edited by P. L. Abbott and W. J. Elliott, San Diego Association of Geologists Guidebook, pp. 17–36.

Fisher, M., 2002. Personal communication.

Geist, E. L., 1998. Local tsunamis and earthquake source parameters, in Tsunamigenic Earthquakes and Their Consequences, *Adv. Geophys.* **39**, 117–209 Academic Press, San Diego.

Geist, E. L., 2002. Complex earthquake rupture and local tsunamis, *J. Geophys. Res., [Space Phys.]* **107**, ESE (May).

Goldfinger, C., 2003. Personal communication.

Goldfinger, C., Huftile, G. J., Legg, M., Yeats, R., and Kamerling, M., 2003. Vertical tectonics at the Peninsular Ranges-Transverse Ranges intersection: Offshore investigations of Pleistocene low-stand shorelines, in American Association of Petroleum Geologists, Pacific Section, Annual Meeting, Long Beach, CA, *Abstracts*.

Goldfinger, C., Legg, M., and Torres, M., 2000. New mapping and submersible observations of recent activity on the San Clemente Fault, *EOS Trans. Am. Geophys. Union* **81**, 1069.

Greene, H. G., and Kennedy, M. P., 1987. Geology of the California continental margin: Explanation of the California continental margin map series, California Division of Mines and Geology, *Bulletin 207*, 110 pp.

Greene, H. G., and Maher, N., 2000. Slope instability and the potential for tsunami generating landslides, *NSF Workshop on the Prediction of Underwater Landslide and Slump Occurrence of Southern California*, Los Angeles, CA.

Gutenberg, B., Richter, C. F., and Wood, H. O., 1932. The earthquake in Santa Monica Bay, California, on August 30, 1930, *Bull. Seismol. Soc. Am.* **22**, 138–154.

Hanks, T. C., 1979. The Lompoc, California, earthquake (November 4, 1927; M=7.3) and its aftershocks, *Bull. Seismol. Soc. Am.* **69**, 451–462.

Hartzell, S. H., and Heaton, T. H., 1983. Inversion of strong ground motion and teleseismic waveform data for the fault rupture history of the 1979 Imperial Valley, California earthquake, *Bull. Seismol. Soc. Am.* **73**, 1553–1583.

Hauksson, E., 1990. Earthquakes, faulting, and stress in the Los Angeles basin, *J. Geophys. Res., [Space Phys.]* **95**, 15365–15394.

Hauksson, E., and Gross, S., 1991. Source parameters of the 1933 Long Beach earthquake, *Bull. Seismol. Soc. Am.* **81**, 81–90.

Hauksson, E., and Jones, L. M., 1988. The July 1986 Oceanside (ML = 5.3) earthquake sequence in the continental borderland, southern California, *Bull. Seismol. Soc. Am.* **78**, 1885–1906.

Hauksson, E., Jones, L. M., and Hutton, K., 1995. The 1994 Northridge earthquake sequence in California: Seismological and tectonic aspects, *J. Geophys. Res., [Space Phys.]* **100**, 12335–12355.

Hauksson, E., and Saldivar, G. V., 1986. The 1930 Santa Monica and the 1979 Malibu, California, earthquakes, *Bull. Seismol. Soc. Am.* **76**, 1542–1559.

Hill, D. P., Eaton, J. P., and Jones, L. M., 1990. Seismicity, 1980–86, chapter 5 in *The San Andreas Fault System, California*, edited by R. E. Wallace, *U.S. Geol. Surv. Prof. Pap. 1515*, 115–151.

Houston, J. R., 1980. Type 19 flood insurance study, Tsunami predictions for southern California, U.S. Army Corps of Engineers Waterways Experiment Station, *Technical Report HL-80-18*, 172 pp.

Imamura, F., Synolakis, C. E., Gica, E., Titov, V., Listanco, E., and Lee, H. J., 1995. Field survey of the 1994 Mindoro Island, Philippines tsunami, *PAGEOPH* **144** (3/4), 875–890.

Junger, A., 1976. Tectonics of the southern California Borderland, in *Aspects of the Geological History of the California Continental Borderland*, edited by D. G. Howell, Pacific Section, American Association of Petroleum Geologists, *Miscellaneous Publication 24*, 486–498.

Kamerling, M., and Luyendyk, B. P., 1979. Tectonic rotations of the Santa Monica Mountains region, western Transverse Ranges, California, suggested by paleomagnetic vectors, *Geol. Soc. Am. Bull.* **90**, 331–337.

King, G. C. P., Stein, R. S., and Lin, J., 1994. Static stress changes and the triggering of earthquakes, *Bull. Seismol. Soc. Am.* **84**, 935–953.

King, G. C. P., Stein, R. S., and Rundle, J. B., 1988. The growth of geological structures by repeated earthquakes: I. Conceptual framework, *J. Geophys. Res., [Space Phys.]* **93**, 13307–13318.

Lajoie, K. R., Ponti, D. J., Powell II, C. L., Mathieson, S. A., and Sarna-Wojcicki, 1992. Emergent marine strandlines and associated sediments, coastal California: A record of Quaternary sea-level fluctuations, vertical tectonic movements, climatic processes, and coastal processes, in *The Regressive Pleistocene Shoreline: Coastal Southern California*, edited by E. G. Heath, and W. L. Lewis, South Coast Geological Society annual field trip guidebook, pp. 81–104.

Lander, J. F., Lockridge, P. A., and Kozuch, M. J., 1993. *Tsunamis Affecting the West Coast of the United States, 1806–1992*, U.S. Dept. Commerce, NOAA, KGRD 29, Boulder, CO, 242 pp.

Larson, K. M., 1993. Application of the Global Positioning System to crustal deformation measurements, 3, Result from the southern California borderlands, *J. Geophys. Res., [Space Phys.]* **98**, 21713–21726.

Lee, W. H. K., Yerkes, R. F., and Simirenko, M., 1979. Recent earthquake activity and focal mechanisms in the western Transverse Ranges, California, U.S. Geological Survey *Circular 799-A*, 1–26.

Legg, M. R., 1985. Geologic Structure and Tectonics of the Inner Continental Borderland Offshore Northern Baja California, Mexico, Ph.D. dissertation, University of California, Santa Barbara, 410 pp.

Legg, M. R., 1991. Developments in understanding the tectonic evolution of the California Continental Borderland, in Osborne, R. H. (Editor), *From Shoreline to Abyss: F. P. Shepard Commemorative Volume*, SEPM Special Publication 46, 291–312.

Legg, M. R., and Agnew, D. C., 1979. The 1862 earthquake in San Diego, in *Earthquakes and Other Perils in the San Diego Region*, edited by P. L. Abbott and W. J. Elliott, San Diego Association of Geologists guidebook, pp. 139–142.

Legg, M. R., and Borrero, J. C., 2001. Tsunami potential of major restraining bends along submarine strike-slip faults, *Proceedings of the International Tsunami Symposium 2001, NOAA/PMEL, Seattle, WA*, pp. 331–342.

Legg, M. R., Einstein, D. E., and Wang, H. D., 1999. Deformation history of a major restraining bend along a right-slip fault: The San Clemente Fault offshore northern Baja California, SCEC Annual Meeting, Palm Springs, CA, *Abstracts*, p. 74.

Legg, M. R., and Kamerling, M. J., 2003. Large-scale basement-involved landslides, California Continental Borderland, *PAGEOPH* **160**, 2033–2051.

Legg, M. R., and Kennedy, M. P., 1991. Oblique divergence and convergence in the California continental borderland, in *Environmental Perils of the San Diego Region*, edited by P. L. Abbott, and W. J. Elliott, San Diego Association of Geologists guidebook, pp. 1–16.

Legg, M. R., Luyendyk, B. P., Mammerickx, J., de Moustier, C., and Tyce, R. C., 1989. Sea beam survey of an active strike-slip fault—The San Clemente Fault in the California continental borderland, *J. Geophys. Res., [Space Phys.]* **94**, 1727–744.

Lindvall, S. C., and Rockwell, T. K., 1995. Holocene activity of the Rose Canyon fault zone in San Diego, California, *J. Geophys. Res., [Space Phys.]* **100**, 24121–24132.

Liu, P. L.-F., Synolakis, C. E., and Yeh, H., 1991. Impressions from the First International Workshop on Long Wave Runup, *J. Fluid Mech.* **229**, 675–688.

Luyendyk, B. P., 1991. A model for Neogene crustal rotations, transtension, and transpression in southern California, *Geol. Soc. Am. Bull.* **103**, 1528–1536.

Ma, K.-F., Satake, K., and Kanamori, H., 1991. The origin of the tsunami excited by the 1989 Loma Prieta earthquake—Faulting or slumping, *Geophys. Res. Lett.* **18**, 637–640.

Magistrale, H., 1993. Seismicity of the Rose Canyon fault zone near San Diego, California, *Bull. Seismol. Soc. Am.* **83**, 1971–1978.

Mann, P., and Gordon, M. B., 1996. Tectonic uplift and exhumation of blueschist belts along transpressional strike-slip fault zones, *Subduction: Top to Bottom*, edited by G. E. Bebout, D. W. Scholl, S. H. Kirby, and J. P. Platt, *American Geophysical Union Monograph* **96**, 143–154.

Marshall, G. A., Stein, R. S., and Thatcher, W., 1991. Faulting geometry and slip from coseismic elevation changes: The 18 October 1989, Loma Prieta, California, earthquake, *Bull. Seismol. Soc. Am.* **81**, 1660–1693.

McCarthy, R. J., Bernard, E. N., and Legg, M. R., 1993. The Cape Mendocino earthquake: A local tsunami wakeup call? *Proceedings of the Eighth Symposium on Coastal and Ocean Management, New Orleans, LA, 19–23 July 1993*, pp. 2812–2828.

McClay, K., and Bonora, M., 2001. Analog models of restraining stepovers in strike-slip fault systems, *AAPG Bull.* **85**, 233–260.

McCulloch, D. S., 1985. Evaluating tsunami potential, *Evaluating Earthquake Hazards in the*

Los Angeles Region—An Earth Science Perspective, edited by J. I. Ziony, *U.S. Geol. Surv. Prof. Pap. 1360*, 375–413.

McNeilan, T. W., Rockwell, T. K., and Resnick, G. S., 1996. Style and rate of Holocene slip, Palos Verdes Fault, southern California, *J. Geophys. Res., [Space Phys.]* **101**, 8317–8334.

Moore, D. G., 1969. Reflection profiling studies of the California Continental Borderland Structure and Quaternary turbidite basins, *Geological Society of America Special Paper 107*, 142 pp.

Morton, D. M., and Matti, J. C., 1993. Extension and contraction within an evolving divergent strike-slip fault complex, The San Andreas and San Jacinto fault zones at their convergence in southern California, *The San Andreas Fault System: Displacement, Palinspastic Reconstruction, and Geologic Evolution*, edited by R. E. Powell, R. J. Weldon, II, and J. C. Matti, *Geological Society of America Memoir 178*, Boulder, CO, 217–230.

Nardin, T. R., and Henyey, T. L., 1978. Pliocene-Pleistocene diastrophism of the Santa Monica and San Pedro shelves, California Continental Borderland, *AAPG Bull.* **62**, 247–272.

Nicholson, C., and Crouch, J. K., 1989. Neotectonic structures along the central and southern California margin, abstract, *Seismol. Res. Lett.* **60**, 23–24.

Okada, Y., 1985. Surface deformation due to shear and tensile faults in a half-space, *Bull. Seismol. Soc. Am.* **75**, 1135–1154.

Okal, E. A., Dengler, L., Araya, S., Borrero, J. C., Gomer, B., Koshimura, S., Laos, G., Olcese, M., Ortiz, M., Swensson, M., Titov, V. V., and Vegas, F., 2002. A field survey of the Camaná, Peru tsunami of June 23, 2001, *Seismol. Res. Lett.* **73**, 904–917.

Pacheco, J., and Nabelek, J., 1988. Source mechanisms of three moderate California earthquakes of July, 1986, *Bull. Seismol. Soc. Am.* **78**, 1907–1929.

Piatanesi, A., Tinti, S., and Gavagni, I., 1996. The slip distribution of the 1992 Nicaragua earthquake from tsunami runup data, *Geophys. Res. Lett.* **23**, 37–40.

Ponti, D. J., and Lajoie, K. R., 1992. Chronostratigraphic implications for tectonic deformation of Palos Verdes and Signal Hills, Los Angeles basin, California, *Proceedings 35th Annual Meeting, Association of Engineering Geologists, Long Beach*, pp. 617–619.

Rivero, C., Shaw, J. H., and Mueller, K., 2000. Oceanside and Thirtymile Bank blind thrusts: Implications for earthquake hazards in coastal southern California, *Geology* **28**, 891–894.

Rockwell, T. K., Lindvall, S., Herzberg, M., Murbach, D., Dawson, T., and Berger, G., 2000. Paleoseismology of the Johnson Valley, Kickapoo, and Homestead Valley faults: Clustering of earthquakes in the Eastern California Shear Zone, *Bull. Seismol. Soc. Am.* **90**, 1200–1236.

Satake, K., and Somerville, P. G., 1992. Location and size of the 1927 Lompoc, California, earthquake from tsunami data, *Bull. Seismol. Soc. Am.* **82**, 1710–1725.

Schwing, F. B., Norton, J. G., and Pilskaln, C. H., 1990. Earthquake and bay: Response of Monterey Bay to Loma Prieta earthquake, *EOS Trans. Am. Geophys. Union* **71**, 250–252.

Seeber, L., and Armbruster, J. G., 1995. The San Andreas fault system through the Transverse Ranges as illuminated by earthquakes, *J. Geophys. Res., [Space Phys.]* **100**, 8285–8310.

Sella, G. F., Dixon, T. H., and Mao, A., 2002. REVEL: A model for recent plate velocities from space geodesy, *J. Geophys. Res., [Space Phys.]* **107**, ETG 11-1–11-31.

Sharp, R. V., 1982. Comparison of 1979 surface faulting with earlier displacements in the Imperial Valley, in *The Imperial Valley, California, Earthquake of October 15, 1979, U.S. Geol. Surv. Prof. Pap. 1254*, 213–222.

Shepard, F. P., and Emery, K. O., 1941. Submarine topography off the southern California coast: Canyons and tectonic interpretation, Geological Society of America *Special Paper 31*, 171 pp.

Sibson, R. H., 1982. Fault zone models, heat flow, and the depth distribution of earthquakes in the continental crust of the United States, *Bull. Seismol. Soc. Am.* **72**, 151–164.

Sibson, R. H., 1985. Stopping of fault ruptures at dilational fault jogs, *Nature (London)* **316**, 248–251.

Sieh, K., Jones, L., Hauksson, E., Hudnut, K., Eberhart-Phillips, D., Heaton, T., Hough, S., Hutton, K., Kanamori, H., Lilje, A., Lindvall, S., McGill, S., Mori, J., Rubin, C., Spotila, J., Stock, J., Thio, H. K., Treiman, J., Wernicke, B., and Zachariasen, J., 1993. Near-field investigations of the Landers earthquake sequence, April to July 1992, *Science* **260**, 171–176.

Sieh, K. E., Stuiver, M., and Brillenger, D., 1989. A more precise chronology of earthquakes produced by the San Andreas Fault in southern California, *J. Geophys. Res., [Space Phys.]* **94**, 603–623.

Stein, R. S., King, G. C. P., and Rundle, J. B., 1988. The growth of geological structures by repeated earthquakes 2, Field examples of continental dip-slip faults, *J. Geophys. Res., [Space Phys.]* **93**, 13319–13331.

Stover and Coffman, 1993. Seismicity of the United States 1568–1989 (revised), *U.S. Geol. Surv. Prof. Pap. 1527*, 418 pp.

Synolakis, C. E., Liu, P. L.-F., Carrier, G., and Yeh, H. H., 1997. Tusnamigenic Seafloor Deformations, *Science* **278**, 598–600.

Synolakis, C. E., Bardet, J.-P., Borrero, J. C., Davies, H. L., Okal, E. A., Silver, E. A., Sweet, S., and Tappin, D. R., 2002. The slump origin of the 1998 Papua New Guinea Tsunami, *Proc. R. Soc. London, Ser. A* **458**, 763–789.

Tadepalli, S., and Synolakis, C. E., 1994. The runup of N-waves, *Proc. R. Soc. London* **445**, 99–112.

Takahashi, To., Takahashi, Ta., Shuto, N., Imamura, F., and Ortiz, M., 1995. Source models for the 1993 Hokkaido Nansei-Oki tsunami, *PAGEOPH* **144**, 747–768.

ten Brink, U. S., Zhang, J., Brocher, T. M., Okaya, D. A., Klitgord, K. D., and Fuis, G. S., 2000. Geophysical evidence for the evolution of the California Inner Continental Borderland as a metamorphic core complex, *J. Geophys. Res., [Space Phys.]* **105**, 5835–5857.

Titov, V., and Gonzalez, F., 1997. Implementation and testing of the method of splitting tsunami (MOST) model, *NOAA Technical Memorandum ERL PMEL-112*.

Titov, V., and Synolakis, C. E., 1995. Modeling of breaking and non-breaking long-wave evolution and runup using VTCS-2., *J. Waterw., Port, Coastal, Ocean Eng.* **121**, 308–316.

Titov, V., and Synolakis, C. E., 1998. Numerical modeling of tidal wave runup, *J. Waterw., Port, Coastal, Ocean Eng.* **124**, 157–171.

Toda, S., Stein, R. S., Reasenberg, P. A., and Dieterich, J. H., 1998. Stress transferred by the M_W=6.5 Kobe, Japan, shock: Effect on aftershocks and future earthquake probabilities, *J. Geophys. Res., [Space Phys.]* **103**, 24543–24565.

Toppozada, R. R., Branum, D., Petersen, M., Hallstrom, C., Cramer, C., and Reichle, M., 2000. Epicenters of and areas damaged by M≥5 California earthquakes, 1800–1999, California Division of Mines and Geology, *Map Sheet 49*, scale 1:562,500.

Toppozada, R. R., Branum, D. M., Reichle, M. S., and Hallstrom, C. L., 2002. San

Andreas fault zone, California: M≥5.5 earthquake history, *Bull. Seismol. Soc. Am.* **92**, 2555–2601.

Toppozada, R. R., Real, C. R., and Parke, D. L., 1981. Preparation of isoseismal maps and summaries of reported effects for pre-1900 California earthquakes, California Division of Mines and Geology, *Open-File Report 81-118AC*, 182 pp.

Treiman, J. A., Kendrick, K. J., Bryant, W. A., Rockwell, R. K., and McGill, S. F., 2002. Primary surface rupture associated with the M_W 7.1 16 October 1999 Hector Mine earthquake, San Bernardino County, California, *Bull. Seismol. Soc. Am.* **92**, 1171–1191.

Tucker, A. Z., and Dolan, J. R., 2001. Paleoseismologic evidence for a>8 ka age of the most recent rupture on the eastern Sierra Madre Fault, northern Los Angeles metropolitan region, California, *Bull. Seismol. Soc. Am.* **91**, 232–249.

U.S. Geological Survey, 1982. *The Imperial Valley, California, Earthquake of October 15, 1979, U.S. Geol. Surv. Prof. Pap. 1254*, 451 pp.

Valensise, G., and Ward, S. N., 1990. Long-term uplift of the Santa Cruz coastline in response to repeated earthquakes along the San Andreas Fault, *Bull. Seismol. Soc. Am.* **81**, 1694–1704.

Vedder, J. G., 1987. Regional geology and petroleum potential of the southern California borderland. in *Geology and Resource Potential of the Continental Margin of Western North America and Adjacent Ocean Basins, Beaufort Sea to Baja California*, edited by D. W. Scholl, A. Grantz, and J. G. Vedder, Circum-Pacific Council for Energy and Mineral Resources, Houston, Texas, Earth Science Series **6**, 403–447.

Vedder, J. G., Beyer, L. A., Junger, Arne, Moore, G. W., Roberts, A. E., Taylor, J. C., and Wagner, H. C., 1974. Preliminary report on the geology of the Continental Borderland of southern California, U.S. Geological Survey, *Miscellaneous Field Studies Map MF-624*, Scale 1:500,000.

Vedder, J. G., Greene, H. G., Clarke, S. H., and Kennedy, M. P., 1986. Geologic map of the mid-southern California continental margin, California Division of Mines and Geology, *California Continental Margin Geologic Map Series*, Area 2 of 7, sheet 1 of 4, scale 1:250,000.

Vedder, J. G., Howell, D. G., and Forman, J. A., 1979. Miocene strata and their relation to other rocks Santa Catalina Island, California, in *Cenozoic Paleogeography of the Western United States*, edited by J. M. Armentrout, M. R. Cole, and H. TerBest, Jr., Society of Economic Paleontologists and Mineralogists, Pacific Coast Paleogeography Symposium **3**, pp. 239–256.

Wald, D. J., and Heaton, T. H., 1994. Spatial and temporal distribution of slip for the 1992 Landers, California, earthquake, *Bull. Seismol. Soc. Am.* **84**, 668–691.

Ward, S. N., and Valensise, G., 1994. The Palos Verdes terraces, California: Bathtub rings from a buried reverse fault, *J. Geophys. Res., [Space Phys.]* **99**, 4485–4494.

Weldon, II, R. J., Meisling, K. E., and Alexander, J., 1993. A speculative history of the San Andreas Fault in the Central Transverse Ranges, California, in The San Andreas Fault system: Displacement, palinspastic reconstruction, and geologic evolution, Boulder, Colorado, edited by R. E. Powell, R. J. Weldon, II, and J. C. Matti, *Geological Society of America Memoir* **178**, 161–198.

Wells, D., and Coppersmith, K., 1994. New empirical relationships among magnitude, rupture length, rupture width, rupture area, and surface displacement, *Bull. Seismol. Soc. Am.* **84**, 974–1002.

PROOF COPY 001403EQS

WGCEP (Working Group on California Eqrthquake Probabilities), 1995. Seismic hazards in southern California: Probable earthqukes, 1994–2024, *Bull. Seismol. Soc. Am.* **85**, 379–439.

White, B. C., 1991. Right-lateral Faulting of Santa Catalina Island, California, Senior thesis, Department of Geological Sciences, San Diego State University, 30 pp.

(Received 25 March 2003; accepted 10 November 2003)